Characterization of the pheophorbide a oxygenase/phyllobilin pathway of chlorophyll breakdown in grasses

Das, Aditi ; Christ, Bastien ; Hörtensteiner, Stefan

Abstract: MAIN CONCLUSION Although the PAO/phyllobilin pathway of chlorophyll breakdown is active in grass leaf senescence, the abundance of phyllobilins is far below the amount of degraded chlorophyll. The yellowing of fully developed leaves is the most prominent visual symptom of plant senescence. Thereby, chlorophyll is degraded via the so-called pheophorbide a oxygenase (PAO)/phyllobilin pathway to a species-specific set of phyllobilins, linear tetrapyrrolic products of chlorophyll breakdown. Here, we investigated the diversity and abundance of phyllobilins in cereal and forage crops, i.e. barley, rice, ryegrass, sorghum and wheat, using liquid chromatography-mass spectrometry. A total of thirteen phyllobilins were identified, among them four novel, not yet described ones, pointing to a rather high diversity of phyllobilin-modifying activities present in the Gramineae. Along with these phyllobilins, barley orthologs of known Arabidopsis thaliana chlorophyll catabolic enzymes were demonstrated to localize in the chloroplast, and two of them, i.e. PAO and pheophytin pheophorbide hydrolase, complemented respective Arabidopsis mutants. These data confirm functionality of the PAO/phyllobilin pathway in grasses. Interestingly, when comparing phyllobilin abundance with amounts of degraded chlorophyll in senescent leaves, in most analyzed grass species only minor fractions of chlorophyll were recovered as phyllobilins, opposite to A. thaliana where phyllobilin quantities match degraded chlorophyll rather well. These data show that, despite the presence and activity of the PAO/phyllobilin pathway in barley (and other cereals), phyllobilins do not accumulate stoichiometrically, implying possible degradation of chlorophyll beyond the phyllobilin level.

DOI: https://doi.org/10.1007/s00425-018-2946-2

Originally published at:
Das, Aditi; Christ, Bastien; Hörtensteiner, Stefan (2018). Characterization of the pheophorbide a oxygenase/phyllobilin pathway of chlorophyll breakdown in grasses. Planta, 248(4):875-892.
DOI: https://doi.org/10.1007/s00425-018-2946-2

Aditi Das, Bastien Christ[1], Stefan Hörtensteiner[2]

Characterization of the pheophorbide *a* oxygenase/phyllobilin pathway of chlorophyll breakdown in grasses

Department of Plant and Microbial Biology, University of Zurich, Zollikerstrasse 107, CH-8008 Zurich, Switzerland

[1]Present address: Whitehead Institute, Massachusetts Institute of Technology, Cambridge, MA 02139-4307

[2]Address correspondence to Stefan Hörtensteiner
email: shorten@botinst.uzh.ch
phone: +41 44 634 82 82
fax: +41 44 634 82 04

Abstract

Main conclusion **Although the PAO/phyllobilin pathway of chlorophyll breakdown is active in grass leaf senescence, the abundance of phyllobilins is far below the amount of degraded chlorophyll.**

The yellowing of fully developed leaves is the most prominent visual symptom of plant senescence. Thereby, chlorophyll is degraded *via* the so-called pheophorbide *a* oxygenase (PAO)/phyllobilin pathway to a species-specific set of phyllobilins, linear tetrapyrrolic products of chlorophyll breakdown. Here, we investigated the diversity and abundance of phyllobilins in cereal and forage crops, i.e. barley, rice, ryegrass, sorghum and wheat, using liquid chromatography-mass spectrometry. A total of thirteen phyllobilins were identified, among them four novel, not yet described ones, pointing to a rather high diversity of phyllobilin-modifying activities present in the Gramineae. Along with these phyllobilins, barley orthologs of known *Arabidopsis thaliana* chlorophyll catabolic enzymes were demonstrated to localize in the chloroplast, and two of them, i.e. PAO and pheophytin pheophorbide hydrolase, complemented respective Arabidopsis mutants. These data confirm functionality of the PAO/phyllobilin pathway in grasses.

Interestingly, when comparing phyllobilin abundance with amounts of degraded chlorophyll in senescent leaves, in most analyzed grass species only minor fractions of chlorophyll were recovered as phyllobilins, opposite to *A. thaliana* where phyllobilin quantities match degraded chlorophyll rather well. These data show that, despite the presence and activity of the PAO/phyllobilin pathway in barley (and other cereals), phyllobilins do not accumulate stoichiometrically, implying possible degradation of chlorophyll beyond the phyllobilin level.

Keywords Chlorophyll breakdown - Chlorophyll catabolite - Gramineae - Phyllobilin - Senescence

Introduction

Senescence is an integral and essential physiological process of plants that is highly coordinated and regulated at the molecular, genetic, cellular and subcellular level (Lim et al. 2007). Of agronomic relevance in many crop species, most of which undergo monocarpic senescence, is senescence of leaves, the key process for the remobilization and translocation of mineral nutrients from leaves to sink organs such as maturing seeds and fruits (Lim et al. 2007; Avice and Etienne 2014; Schiltz et al. 2005; Distelfeld et al. 2014). Thus, since many years, leaf senescence is under the limelight of scientific research for a better understanding of the underlying regulatory mechanisms to be targeted for crop improvement (Distelfeld et al. 2014; Gregersen et al. 2013). Among many metabolic reactions that take place in a leaf during senescence, loss of chlorophyll is its most visible symptom.

Chlorophyll is broken down *via* the pheophorbide *a* oxygenase (PAO)/phyllobilin pathway (Kräutler and Hörtensteiner 2014), which to date is best elucidated in the dicot model plant *Arabidopsis thaliana* (Arabidopsis) (Kuai et al. 2018). The pathway is comprised of sequential enzymatic reactions catalyzed by chlorophyll catabolic enzymes (CCEs) and can be divided into two parts (Fig. 1). The first part commences with the conversion of chlorophyll *b* to chlorophyll *a* that is catalyzed in a two-step reaction by chlorophyll *b* reductase and 7-hydroxy-chlorophyll *a* reductase (HCAR) (Meguro et al. 2011; Tanaka and Tanaka 2011). The Arabidopsis genome encodes two chlorophyll *b* reductases, i.e. non-yellow coloring 1(NYC1) and NYC1-like (NOL) (Kusaba et al. 2007; Horie et al. 2009). The pathway proceeds by the removal of Mg by stay-green protein (SGR) (Shimoda et al. 2016), yielding pheophytin *a*. In Arabidopsis, three SGR genes are present, i.e. *SGR1*, *SGR2* and *SGR-like* (*SGRL*) (Hörtensteiner 2009; Sakuraba et al. 2014; Wu et al. 2016). Dephytylation, i.e. removal of the phytol chain, is the next step in the pathway and is of great significance, because cleavage of the hydrophobic ester bond increases the solubility of the further breakdown products. This step is catalyzed by pheophytin pheophorbide hydrolase (PPH) (Schelbert et al. 2009; Morita et al. 2009; Ren et al. 2010) and yields the highly phototoxic intermediate pheophorbide *a*. Subsequently, the chlorin macrocycle of pheophorbide *a* is oxygenolytically opened by PAO between rings D and A (see Fig. 1, for ring and atom numbering) forming red chlorophyll catabolite (RCC) (Hörtensteiner et al. 1995; Pružinská et al. 2003). RCC is a photoactive linear

tetrapyrrole that is rapidly channeled through red chlorophyll catabolite reductase (RCCR) reducing the conjugated C15/C16 double bond and yielding a colorless product, *primary* fluorescent chlorophyll catabolite (*p*FCC; Fig. 1) (Rodoni et al. 1997; Mühlecker et al. 1997; Pružinská et al. 2007). Formation of *p*FCC inside senescing chloroplasts terminates the first part of the PAO/phyllobilin pathway.

The second phase of the pathway comprises different side chain modifications of *p*FCC that help increasing the polarity of the catabolites for their final storage in the vacuole (Christ and Hörtensteiner 2014). Most of these modifications occur in a species-specific manner and outside the plastid, except C3^2-hydroxylation that has recently been shown to be catalyzed by translocon at the inner chloroplast envelope 55 (TIC55), an inner chloroplast envelope-localized Rieske type oxygenase, and that occurs in all higher plant species investigated with respect to the formation of phyllobilins so far (Hauenstein et al. 2016). Thus, this reaction was recently considered to belong to part 1 of the PAO/phyllobilin pathway (Kuai et al. 2018). Prominent further modifications of *p*FCC are (i) demethylation of the C8^3-carboxymethyl ester, which in Arabidopsis is catalyzed by methylesterase 16 (MES16) (Christ et al. 2012), (ii) C3^2-OH glucosylation and/or malonylation (Hörtensteiner 1998), and (iii) C18-vinyl group dihydroxylation, which does not occur in Arabidopsis (Christ et al. 2016). In Arabidopsis, cytochrome P450 monooxygenase (CYP) CYP89A9 was recently shown to catalyze the oxidative removal of the formyl group at the C1 position of *p*FCC (Christ et al. 2013), thus, converting formyloxobilin-type linear fluorescent chlorophyll catabolites (FCCs) that are directly derived from *p*FCC, into dioxobilin-type linear fluorescent chlorophyll catabolites (DFCCs; Fig. 1) (Kräutler 2014). As the final step of chlorophyll breakdown, FCCs and DFCCs are imported into the vacuole, where they are rapidly isomerized under the acidic vacuolar pH (Oberhuber et al. 2003; Oberhuber et al. 2008) to respective nonfluorescent catabolites, i.e. formyloxobilin-type nonfluorescent chlorophyll catabolites (NCCs) and dioxobilin-type nonfluorescent chlorophyll catabolites (DNCCs) (Kräutler 2014).

In the past, about 30 structurally distinct NCCs and DNCCs have been identified from more than 20 plant species (Kräutler 2016; Kuai et al. 2018); interestingly however, only two monocot species, i.e. barley and maize, have been analyzed so far (Kräutler et al. 1991; Berghold et al. 2006; Losey and Engel 2001). While in senescent leaves of Arabidopsis and *Cercidiphyllum japonicum* the abundance of phyllobilins has been shown to well correlate with the amounts of degraded chlorophyll (Christ et al. 2013; Curty and Engel 1996), the so

far identified one NCC (termed *Hv*-NCC-1) and one DNCC (termed *Hv*-UCC-1) of barley together only represented about 20% of the expected chlorophyll catabolites (Losey and Engel 2001). In addition, induction of leaf senescence after specific ^{14}C-labeling of chlorophyll in barley identified several different radiolabeled compounds (Peisker et al. 1990), indicating that additional, as yet structurally unidentified catabolites accumulate in this species.

The aim of this work was to explore the diversity of phyllobilin formation in monocot species and to elucidate to what extent the established PAO/phyllobilin pathway that has nearly exclusively been studied in dicots so far is also conserved and active within monocots Our work, that primarily focused on barley, indeed confirms the identity and operation of key CCEs in monocots. In addition, we demonstrate that phyllobilin-modifying activities are rather diverse within the Gramineae and that in most investigated species, phyllobilins accumulate to abundances far below than expected when compared to the amounts of degraded chlorophyll.

Material and methods

Plant materials and growth conditions

Different varieties from each of the plant species *Hordeum vulgare* [var. Golden Promise (GP) and Baraka (BA)], *Triticum aestivum* [var. Chinese Spring (CS), Chancellor (CH), Kanzler (KA) and Bobwhite (BW)], *Lolium perenne* [var. Ceres (CE)], *Oryza sativa* [var. Nipponbare (NB)] and *Sorghum bicolor* [var. E-Tian (ET)] were propagated in Conviron growth chambers equipped with 400 Watt pulse start lamps (Conviron, Winnipeg, Canada). Barley, wheat, sorghum and rice were grown under long day conditions (500-600 μmol photons $m^{-2}s^{-1}$) but with different temperature and humidity preferences [22°C (day); 16°C (night), 60% relative humidity for barley and wheat; 28°C (day); 22°C (night), 50% relative humidity for sorghum and 28°C (day); 24°C (night) 75% relative humidity for rice]. Ryegrass was grown in a controlled-environment chamber (12 h light and 12 h dark at constant temperature of 22°C and 60% relative humidity). For Arabidopsis, Columbia-0 (Col-0) was used as wild type. *pao1* and *pph-1* have been described (Pružinská et al. 2005; Schelbert et al. 2009). Arabidopsis

plants were grown either in 12 h light/12 h dark (12/12 h) or 8 h light/16 h dark (short-day) growth chambers equipped with fluorescent light of an intensity of 60-120 μmol photons m^{-2} s^{-1} at 22°C and 60% relative humidity.

Senescence induction and 2,2'-bipyridyl treatment

To induce senescence in monocots, detached primary leaves of ten-days-old plants were incubated on wet filter paper in dark cabinets at ambient temperature for up to 8 days. Likewise, true leaves number 7-9 (Farmer et al. 2013) of five-weeks-old (12/12 h-grown) plants were used for senescence induction in Arabidopsis.

For CO or $^{18}O_2$ experiments, leaves number 7-9 of eight-weeks-old (short-day-grown) Arabidopsis Col-0 plants, primary leaves of ten-days-old barley var. Golden Promise and ryegrass var. Ceres were dark-incubated for 6 d in an exicator containing carbon monoxide (CO) (PanGas AG, Dagmersellen, Switzerland) mixed with ambient air [0% or 50% (v/v)] or with $^{18}O_2$ [97% (v/v)] (Campro Scientific, Berlin, Germany).

For 2,2'-bipyridyl treatments, ten-days-old primary leaves of barley var. Golden Promise were placed on filter paper soaked with distilled water. After 3 days in darkness at ambient temperature, half of the leaves were transferred to filter paper soaked with 0.1 mM 2,2'-bipyridyl (Sigma-Aldrich, Buchs, Switzerland). The other half (control) was transferred to fresh water-soaked filter paper, and leaves incubated in darkness for another 5 d.

Biocomputational methods

Barley and rice CCEs were identified by BLASTP searches (Altschul et al. 1997) at the National Center for Biotechnology Information (http://www.ncbi.nlm.nih.gov) using respective Arabidopsis CCEs. For determining protein identity and similarity (Suppl. Fig. S3), proteins were aligned using Clustal Omega (https://www.ebi.ac.uk/Tools/msa/clustalo/). Similarity and identity scores were then calculated based on the alignment using the 'Ident and Sim' utility (http://www.bioinformatics.org/sms2/ident_sim.html) (Stothard 2000) with default similarity group settings. Graphical outputs of protein alignments (Suppl. Figs. S3 and S4) were produced using Gendoc (http://genedoc.software.informer.com/).

GFP fusion protein analysis

Full-length cDNA clones of barley var. Haruna nijo CCEs (Matsumoto et al. 2011) were obtained from the National Institute of Agrobiological Sciences (Ibaraki, Japan). The GenBank ID of the clones are listed in Suppl. Table S1. They were amplified by PCR with KAPA HiFi HotStart DNA polymerase (Kapa Biosystems, Baden, Switzerland) using primers carrying appropriate restriction sites at the ends (Suppl. Table S2). The PCR fragments were cloned into pGEM-T Easy (Promega, Dübendorf, Switzerland) and, after restriction digest, subcloned into pUC18-spGFP6 (Meyer et al. 2006), thereby producing protein fusions with C-terminally located GFP.

Protoplasts were isolated from ten-days-old barley leaves. For this, cell wall digestion was performed as published (Rentsch and Martinoia 1991) and protoplasts subsequently purified (Bai et al. 2014). Cell numbers were quantified with a Neubauer counting chamber and adjusted to 4 x 10^6 protoplasts ml^{-1}. Protoplasts were transformed using 20% polyethylene glycol (Meyer et al. 2006). After incubation in the dark for 48 h at room temperature, protoplasts were analyzed by laser scanning confocal microscopy (SP5; Leica Microsystems, Heerbrugg, Switzerland). GFP fluorescence was imaged at an excitation wavelength of 488 nm and the emission signal was recovered between 495 and 530 nm. Detection of chlorophyll autofluorescence was at 730 nm.

RNA isolation and real-time quantitative PCR (qPCR)

RNA was isolated using the RNeasy Plant Mini Kit (Qiagen, Hombrechtikon, Switzerland) with the following changes. The supernatant of the flow-through obtained after centrifugation of the plant lysate using the lilac QIAshredder spin columns, 250 µL each of water-saturated phenol and a 24:1 (v/v) mixture of chloroform:isoamylalcohol were added. After vigorous vortexing, the mixture was centrifuged at 16,000×*g* for 5 min at 4°C. To the upper aqueous phase, two volumes of chloroform:isoamylalcohol [24:1 (v/v)] were added, followed by vortexing and centrifugation as before. The upper aqueous phase was mixed with an equal volume of ethanol and immediately transferred to the pink RNeasy spin column. Thereafter, the provided protocol of the kit was followed. RNA was quantified using a Nanodrop 1000 spectrophotometer (Thermo Fischer Scientific, Dietikon, Switzerland). One µg of RNA was used for the synthesis of first strand cDNA using Moloney murine leukemia virus reverse transcriptase and oligo $(dT)_{15}$ primers after DNAse treatment (Promega, Dübendorf, Switzerland).

For qPCR studies, three biological and each three technical replicates of each samples were analyzed. For quantification, SYBR Green master mix (Thermo Fischer Scientifc) was used to run qPCR on a 7500 Fast Real-time PCR system (Life Technologies, Zug, Switzerland). The gene-specific primers used for qPCR analysis are listed in Suppl. Table S2. *HvS40* (Krupinska et al. 2002) and *ADP* (Ferdous et al. 2015) were used as senescence control and housekeeping control genes, respectively. Expression levels were normalized to the expression of *ADP* using the delta-delta Ct method (Livak and Schmittgen 2001).

Complementation tests

Full-length cDNA sequences of *HvPPH* and *HvPAO* were amplified using KAPA HiFi HotStart DNA polymerase (Kapa Biosystems) and the primers listed in Suppl. Table S2. After cloning into pGEM-T Easy (Promega) and excision with *Xho*I and *BamH*I (for *HvPPH*) or *Hin*dIII (for *HvPAO*), the amplicons were sub-cloned into pHannibal (Wesley et al. 2001) containing the cauliflower mosaic virus 35S double enhancer promoter and an octopine synthase terminator. Constructs were finally cloned into pGreen 0029 (Hellens et al. 2000) via *Not*I sites. After verification by sequencing, the constructs were transformed into *Agrobacterium tumefaciens* strain GV3101 along with pSOUP (Hellens et al. 2000). Arabidopsis *pph-1* and *pao1* mutant plants were transformed with the floral dip method (Clough and Bent 1998). The transformants, named *pph-1*/35S:*Hv*PPH and *pao1*/35S:*Hv*PAO*,* respectively, were selected on ½ MS plates containing kanamycin. Homozygosity for the original T-DNA insertion of *pph-1* and *pao1* was verified in T2 plants using the gene-specific RP and LP primers and the T DNA-specific primer LBb1.3 listed in Suppl. Table S2.

Extraction and analysis of chlorins

For the extraction of chlorins, leaf tissue was homogenized in liquid nitrogen and 3-fold (v/w) extraction buffer [90% acetone, 10% (v/v) Tris-HCl; pH = 8.0, pre-cooled to -20°C] was added. The samples were sonicated in an ice-cooled ultrasound bath in the dark at 4°C for 10 min (Das et al. 2018). After centrifugation at 16,000×*g* for 2 min, supernatants were divided into two fractions, i.e. for spectrophotometric determination of chlorophyll concentrations (Strain et al. 1971) using a DU-800 UV/Vis spectrophotometer (Beckman Coulter, Nyon, Switzerland), and for the analysis of pheophorbide and pheophytin *a* by reversed-phase HPLC-equipped with a photodiode array detector (Dionex PDA-100, Thermo Fisher Scientific) (Christ et al.

2012) using established elution conditions (Langmeier et al. 1993). Peaks were analyzed and quantified with authentic standards (Guyer et al. 2018) using Chromeleon (Thermo Fisher Scientific).

Extraction and analysis of phyllobilins

Leaf material, collected in tubes containing glass beads, was shock-frozen in liquid nitrogen and phyllobilins extracted following published procedures (Christ et al. 2016; Hauenstein et al. 2016). Samples were analyzed on a liquid chromatography (LC)-mass spectrometry (MS) system (LC-MS) composed of an ultrahigh performance LC (Dionex Ultimate 3000, Thermo Fisher Scientific) and an electrospray ionization-quadrupole-time of flight mass spectrometer (Compact, Bruker Daltonics, Bremen, Germany). Phyllobilins were detected by comparing senescent versus green leaf samples and screening for typical fragmentation features of known phyllobilins as outlined elsewhere (Christ et al. 2016). This screening was accompanied by analysis of typical UV/Vis spectral properties of different classes of phyllobilins (Kräutler 2014). MS and MS/MS spectra of all phyllobilins were compiled in a mass spectral library using LibraryEditor (Bruker Daltonics) that also contains the phyllobilins identified in Arabidopsis before (Christ et al. 2016). This Bruker MS library is available on our website (http://www.botinst.uzh.ch/en/research/physiology/horten/ms-library.html) together with the individual MS and MS/MS spectra of all phyllobilins that can be integrated into library databases on other mass spectrometry platforms. The library was used for the identification and determination of relative abundance of each phyllobilin in the samples analyzed here based on the 'Find Molecular Features' algorithm of DataAnalysis (Bruker Daltonics) (Christ et al. 2016). For absolute quantification, *Cj*-NCC-1 (m/z 645.29) was used as phyllobilin standard (Moser et al. 2008). Reliability of 'molecular feature'-based phyllobilin quantification has been demonstrated for Arabidopsis by comparing it with UV-absorption-based quantification (Christ et al. 2016). Similar results were obtained with the phyllobilins analyzed here from different grass species.

Expression of recombinant *Hv*PPH

MBP-ΔPPH of Arabidopsis (MBP-Δ*At*PPH) has been described elsewhere (Schelbert et al. 2009). For cloning of MBP-Δ*Hv*PPH_1 (F118/H261), a truncated *HvPPH* fragment devoid of the sequence encoding the predicted chloroplast transit peptide was amplified from cDNA

clone NIASHv2029B03 (Matsumoto et al. 2011) using KAPA HiFi HotStart DNA polymerase (Kapa Biosystems) and the primers listed in Suppl. Table S2. To produce MBP-Δ*Hv*PPH (S118/P261), three overlapping partial PCR fragments containing the respective changes were produced from cDNA clone NIASHv2029B03 with the primers listed in Suppl. Table S2. In a second PCR reaction, these fragments were combined to yield Δ*Hv*PPH. After digestion with *BamH*I and *Sal*I (Suppl. Table S2), amplicons were cloned into pMal-c2 vector (New England Biolabs, Allschwil, Switzerland) and transformed into *E. coli* BL21 (DE3) (New England Biolabs). Recombinant protein expression and PPH activity assays were carried out as described (Schelbert et al. 2009; Guyer et al. 2014).

Protein extraction and immunoblot analysis

Soluble and membrane protein fractions were produced from liquid nitrogen-grinded leaf material as described (Schenk et al. 2007). For SDS PAGE and immunoblot analysis, proteins were loaded based on equal amounts of fresh weight (leaf material) or cell culture (recombinant expression of PPH). SDS-pages were stained with Commassie brilliant blue. Anti-PAO (mouse-monoclonal, 1:500; Gray et al. 2004) and anti-MBP (mouse-monoclonal, 1:10,000; New England Biolabs) antibodies were used for immunoblot analysis and blots were developed with HRP-conjugated secondary antibodies (rabbit anti-mouse IgG, 1:100,000; Sigma-Aldrich, Buchs, Switzerland) and by chemiluminescence using Immun-Star WesternC kit (Bio-Rad Laboratories, Cressier, Switzerland), and visualized with a Chemidoc XRS gel-documentation system (Bio-Rad Laboratories).

Results

Confirmation of the PAO/phyllobilin pathway identity in barley

Analysis of phyllobilins in barley

LC-MS analysis of chlorophyll catabolites (Rios et al. 2014; Rios et al. 2016), which was recently established in our lab (Christ et al. 2016), was used for a detailed analysis of phyllobilins that occur in senescent leaves of barley. Identified phyllobilins are described following the

classifying nomenclature recently proposed (Christ et al. 2016; Kuai et al. 2018) that indicates the type of phyllobilin (NCC or DNCC), followed by its monoisotopic molecular mass, but ignores the species origin as well as isomeric properties, as for example regarding the isomeric configuration at C16 (Oberhuber et al. 2008). Information about all phyllobilins identified in this work is summarized in Table 1. Table 1 also shows alternative names used in the past for already known phyllobilins. Using two different varieties and combining MS with tandem MS (MS/MS) fragment pattern analysis (Christ et al. 2016) (see Fig. 2 and Suppl. Fig. S1), a total of four DNCCs and seven NCCs could be identified in senescent barley leaves. Besides the already described *Hv*-NCC-1 (NCC_678) (Kräutler et al. 1991) and *Hv*-UCC-1 (DNCC_666) (Losey and Engel 2001), these include five further phyllobilins whose constitutions have been elucidated in the past from other plant species, i.e. DNCC_632-3, DNCC_828, NCC_806, NCC_840 and NCC_892 (Table 1). The other three phyllobilins, i.e. DNCC_650, NCC_662 and NCC_926, were novel.

All barley phyllobilins had an intact $C8^2$-carboxymethyl group, indicating that barley does not possess an ortholog of Arabidopsis MES16, responsible for demethylation in the latter (Christ et al. 2012). In addition, while Arabidopsis phyllobilins are characterized by the exclusive presence of a vinyl group at C18, the majority of the barley phyllobilins are dihydroxylated at this position (see below). To establish whether the, as yet unknown, activity responsible for dihydroxylation requires molecular oxygen, we performed oxygen labeling studies, by inducing barley leaf senescence in the presence of $^{18}O_2$. Previous studies have shown that several enzymes involved in the PAO/phyllobilin pathway, i.e. PAO, CYP89A9 and TIC55 (Christ et al. 2013; Hauenstein et al. 2016; Hörtensteiner et al. 1998) use molecular oxygen, thus cause labeling of the $O1^2$ (in NCCs), $O1^1$ (in DNCCs) and the $O8^3$ position. Senescence induction of barley var. Golden Promise in an $^{18}O_2$ atmosphere caused incorporation of up to four labeled oxygen atoms, exemplified for the C18-dihydroxylated phyllobilins DNCC_666 and the NCC_678 (**Fig. 3**). On one hand, this indicates that chlorophyll breakdown in barley likely involves enzymes that are functionally identical to the respective Arabidopsis enzymes, such as PAO and TIC55; on the other hand, it demonstrated that both oxygen atoms present in the $C18^1$ and $C18^2$ hydroxyl groups are derived from molecular oxygen.

Comparison of LC-MS base peak chromatograms (BPCs) with the extracted ion

chromatograms (EICs) representing the pseudo-molecular ions of all phyllobilins found in each barley variety (Suppl. Fig. S2) uncovered that phyllobilins produced rather intense MS signals in senescent barley leaf samples using our experimental set-up. Respective peaks were absent in the extracts of green leaf tissues, indicating them to be specifically produced during senescence. In both analyzed barley varieties, the two most abundant phyllobilins were DNCC_666 and NCC_678, i.e. the only two phyllobilins previously identified in this species (Kräutler et al. 1991; Losey and Engel 2001). This indicated that the experimental LC-MS set-up used here was capable in identifying low abundant phyllobilins with high sensitivity.

Identification and experimental verification of barley CCEs orthologs

To identify potential orthologs of the Arabidopsis CCEs that are involved in reactions of the first part of the PAO/phyllobilin pathway, i.e. NYC1, NOL, SGR, PPH and PAO (see Fig. 1), in barley and rice, BLASTP searches were performed at NCBI (http://blast.ncbi.nlm.nih.gov). Overall protein sequence identities were between 60% and 90% (Suppl. Fig. S3**a**). Multiple amino acid sequence alignments for PAO and PPH (Suppl. Figs. S3**b** and S4**a**) show that conserved motifs, i.e. a Rieske-type iron-sulfur center and a mononuclear iron center (Gray et al. 2004; Pružinská et al. 2003), were present in the barley and rice PAO candidates (Suppl. Fig. S3**a**), while a PPH domain that harbors the active-site serine residue defining *At*PPH as a serine esterase (Schelbert et al. 2009; Guyer et al. 2018) was also present in the barley and rice PPH candidates (Suppl. Fig. S4**a**).

A closer look into the BLAST output sequences of *Hv*PPH revealed some ambiguity concerning *PPH* gene identity in barley, i.e. two different sequences, tentatively named *Hv*PPH_1 (Genbank accession BAK02426.1) and *Hv*PPH_2 (Genbank accession BAJ96082.1). Both accessions were different to *Hv*PPH (HORVU7Hr1G083370.9) predicted from the published barley genome draft (Mascher et al. 2017). *Hv*PPH_2 contained a truncated C-terminus as compared to *Hv*PPH and *Hv*PPH_2, while *Hv*PPH_1 contained a phenylalanine residue at position 118 (F118) and a histidine residue at position 261 (H261) as compared to a serine (S118) and a proline residue (P261), respectively, in *Hv*PPH and *Hv*PPH_2 (Suppl. Fig. S4**a**). These amino acid changes result from single nucleotide differences (T/C and A/C, respectively) between *Hv*PPH_1 and *Hv*PPH_2/*Hv*PPH. Information from more than 30 expressed sequence tags (ESTs) indicated major support for S118/P261 and the long C-

terminus version (Suppl. Fig. S4**b**), i.e. the features present in *Hv*PPH predicted from the published barley genome. To test *in vitro* PPH activity, truncated versions of *Hv*PPH (S118/P261; named MBP-Δ*Hv*PPH) and *Hv*PPH_1 (F118/H261; named MBP-Δ*Hv*PPH_1) that were devoid of the predicted chloroplast transit peptide, were fused to maltose binding protein (MBP) and expressed in *E. coli*. The recombinant proteins were found to be located in the soluble cell fraction as determined by SDS-PAGE and Western blot analysis (Suppl. Fig. S4**c**-**d**). Surprisingly, MBP-Δ*Hv*PPH_1 was unable to produce pheophorbide *a* from pheophytin *a* as substrate*,* while MBP-Δ*Hv*PPH was able to dephytylate pheophytin *a*, like recombinant MBP-Δ*At*PPH (Suppl. Fig. S4**e**). This indicated that serine 118 and/or proline 261 play an important role for PPH activity, despite the fact that they lie outside the PPH motif (Suppl. Fig. S4**a**) and distant from the residues constituting the catalytic triad or the oxyanion hole of PPH, as recently determined for the Arabidopsis protein (Guyer et al. 2018). *Hv*PPH was used for all further experiments.

Based on ChloroP prediction (Emanuelsson et al. 1999) all identified *Hv*CCE candidates were predicted to localize to the chloroplast. To verify this experimentally, C-terminal green fluorescent protein (GFP) fusions were created and analyzed in mesophyll protoplasts of barley var. Golden Promise using confocal microscopy. All fusion proteins distinctly localized to chloroplasts, i.e. largely co-localized with chlorophyll autofluorescence (Fig. 4) confirming that, like in Arabidopsis (Sakuraba et al. 2012), these CCEs are targeted to either the thylakoid membrane or the stroma.

Identity of *Hv*PAO and *Hv*PPH as orthologs of the respective Arabidopsis CCEs was confirmed by their ability to functionally complement the phenotypes of respective Arabidopsis knockout mutants (Pružinská et al. 2005; Schelbert et al. 2009). To this end, *HvPAO* and *HvPPH* cDNAs were expressed in *pao1* and *pph-1*, respectively, under the control of the 35S promoter and plants analyzed in the second generation after transformation. Detached leaves from *pao1*/35S:*Hv*PAO (Fig. 5A) and *pph-1*/35S:*Hv*PPH (Fig. 5B) lost chlorophyll under dark-induced senescence as wild type Arabidopsis. In addition, HPLC analysis demonstrated absence of pheophorbide *a* (Fig. 5C) or pheophytin *a* (Fig. 5D) in the respective *Hv*CCE-expressing mutant lines, confirming the identity of *Hv*PAO and *Hv*PPH as genuine barley CCEs of the PAO/phyllobilin pathway.

To further verify the *in vivo* involvement of PAO in the breakdown of chlorophyll in barley, senescence was induced in the presence of the iron-chelator 2,2'-bipyridyl, which earlier has been shown in canola (*Brassica napus*) to slow down chlorophyll breakdown at the level of PAO (Hörtensteiner et al. 1995). After 8 d in the dark, 2,2'-bipyridyl-treated leaves retained visibly more chlorophyll than the control (Fig. 6A). HPLC analysis confirmed the retention of chlorophyll in these samples and also showed that the treated samples accumulated considerable amounts of pheophorbide *a* (Fig. 6B), confirming the involvement of PAO, an iron-containing enzyme, in the chlorophyll breakdown process in barley. Finally, expression of the genes encoding the barley CCEs was analyzed by real-time quantitative RT-PCR in the Golden Promise variety after senescence induction of detached primary leaves for 0, 4 and 8 d (Fig. 6C). *Hv*S40, a known senescence associated gene in barley (Krupinska et al. 2002) was used as a positive control. Among the invested genes encoding *Hv*CCEs, *NYC1*, *PPH*, *PAO* expression increased with the progression of senescence, while *SGR* was only slightly upregulated and the expression of *NOL* did not change. In line with an upregulation of *PAO*, PAO protein abundance increased with senescence progression (Fig. 6D). In summary, our data confirmed that at least the first part of the PAO/phyllobilin pathway that is well-established to be active in Arabidopsis similarly or identically functions in barley.

Analysis of phyllobilin diversity in grasses

As detailed above, the phyllobilin composition of barley varieties largely differs from that of Arabidopsis indicating major differences in the presence or activity of enzymes catalyzing the reactions of the second part of the PAO/phyllobilin pathway. To further explore these differences within the Gramineae, we extended our LC-MS analysis to a variety of grass crops, i.e. wheat (four varieties), ryegrass, sorghum, and rice (see Suppl. Figs. S5 and S6, for BPC and EIC of respective phyllobilins in each species). As evident from Table 1, phyllobilin composition was generally similar, but less complex than in barley. Thus, all identified phyllobilins contained an intact $C8^2$ carboxymethyl ester, indicating that Gramineae generally are devoid of a MES16-like activity. Furthermore, all species produced C18-dihydroxylated phyllobilins. Nevertheless, the analysis of ryegrass var. Ceres identified two additional DNCCs, i.e. DNCC_794 that is also present in Arabidopsis *mes16* mutants (Christ et al. 2016) and the novel DNCC_880 (Table 1; see Suppl. Fig. S1, for respective MS and MS/MS spectra). Further

differences between the species were evident when comparing relative abundances of NCCs vs DNCCs (Fig. 7A). Barley accumulated more DNCCs than NCCs, while it was the opposite in all four investigated wheat varieties. By contrast, ryegrass and sorghum almost exclusively produced DNCCs and NCCs, respectively. This indicated major differences among the species in the activity/identity of the respective deformylation reaction. However, these differences did not correlate with the phylogenetic relationship between the investigated species (Soreng et al. 2015). In Arabidopsis, DNCC formation requires CYP89A9 (Christ et al. 2013) and has been shown to be inhibited by CO, a potent inhibitor of CYPs (Schuler 1996). To test whether also in grasses DNCC formation depends on a CYP activity, we investigated phyllobilin formation in barley var. Golden Promise and ryegrass var. Ceres under a CO-containing atmosphere (Fig. 7B). Surprisingly, relative abundance of DNCCs was unaltered in the grasses, while CO treatment reduced relative DNCC abundance in Arabidopsis, as has been shown before (Christ et al. 2013).

In grasses, stoichiometry between degraded chlorophyll and phyllobilins is mismatched.

It was shown for Arabidopsis that a large proportion of 70-90% of the degraded chlorophyll in senescent leaves is recovered in phyllobilins (Christ et al. 2013; Christ et al. 2016). To investigate this in grasses, we used LC-MS analysis (Christ et al. 2016) to quantify phyllobilins after 8 d of dark incubation and correlated the obtained values to the amounts of chlorophyll degraded within the same time using the same plant material. Chlorophyll contents significantly decreased in each tested species (Suppl. Fig. S7). However, the abundance of phyllobilins was not proportional to the amount of degraded chlorophyll (Fig. 7C). Except for ryegrass where more than 60% of the degraded chlorophyll was recovered in phyllobilins, phyllobilins accounted for only 30% or less in all other investigated species. Particularly drastic were the results for sorghum and rice where only 6% and less than 2%, respectively, of chlorophyll was recovered in phyllobilins. Interestingly, in senescent flag leaves of field-grown barley var. Carina, phyllobilins were entirely absent (data not shown).

Discussion

The prevailing aim of leaf senescence is the remobilization of valuable nutrients, primarily nitrogen and phosphorous, to sink organs such as seeds (Lim et al. 2007). All agronomically relevant monocot crops studied here are annuals. Thus, understanding the processes and regulatory mechanisms of monocarpic senescence in these crops is of particular interest, because it is widely accepted that modulation of leaf senescence may impact crop yield (Uauy et al. 2006; Distelfeld et al. 2014; Gregersen et al. 2013). However, as a key feature for an intermittent grazing management for cattle ranching, leaf senescence is also relevant in perennial forage crops, such as ryegrass (Fulkerson and Donaghy 2001).

The phenotypic loss of chlorophyll is an integral aspect of leaf senescence (Ougham et al. 2008) and the importance of chlorophyll degradation is obvious from the phenotype of mutants that are deficient in chlorophyll breakdown. For example, the maize *lls1* mutant that is deficient in PAO exhibits a premature cell death that ultimately kills the entire plant (Gray et al. 2002). Similarly, rice *PAO* knockdown lines show a cell death phenotype (Tang et al. 2011). Despite its obvious importance, the PAO/phyllobilin pathway of chlorophyll breakdown has been investigated in mainly two monocot species so far, i.e. in rice, a cereal crop (Tang et al. 2011; Kusaba et al. 2007; Jiang et al. 2007), and in ryegrass, a forage crop (Jespersen et al. 2016; Zhang et al. 2016). The aim of this work was to shed more light on the mechanism of chlorophyll breakdown in monocot crops. To induce senescence, detached leaves were incubated in the dark. This approach has been widely used in many species and, although being rather artificial and uncoupling visual senescence from actual remobilization processes, it was shown that chlorophyll breakdown, including the expression of genes encoding CCEs, is comparable between different ways of leaf senescence induction, i.e. developmental senescence or dark incubation of either detached leaves (used here), individual attached leaves, or entire plants (Buchanan-Wollaston et al. 2005; Breeze et al. 2011; Van der Graaff et al. 2006; Zhang et al. 2014).

Using an array of molecular, biochemical and analytical methods, we confirm that the principle components of the PAO/phyllobilin pathway, specifically the reactions of the first part of the pathway that are required to convert chlorophyll to *p*FCC are present and active in barley, the main model species used in this work. We identified highly homologous barley sequences of the major CCEs, i.e. NYC1, NOL, SGR, PPH and PAO, whose biochemical functions were first identified in Arabidopsis [PPH (Schelbert et al. 2009); PAO (Pružinská et al. 2003; Tanaka et al. 2003); SGR (Shimoda et al. 2016)] or rice [NYC1 and NOL (Kusaba et al. 2007)].

These barley CCEs were characterized with regard to gene expression and subcellular localization and with overall confirmation of data known from Arabidopsis. Thus, like their Arabidopsis orthologs (Sakuraba et al. 2012), all five investigated barley CCEs localize to chloroplasts. In addition, barley *NYC1*, *SGR*, *PPH* and *PAO* are transcriptionally up-regulated upon senescence-induction in the dark as has been shown for respective Arabidopsis and rice genes (Schelbert et al. 2009; Pružinská et al. 2003; Kusaba et al. 2007; Park et al. 2007). Like described for its ortholog in Arabidopsis (Sakuraba et al. 2013) but distinct to rice (Kusaba et al. 2007), *HvNOL* expression remained unchanged during senescence. It has been proposed for Arabidopsis that NOL is involved in chlorophyll turnover at steady state rather than during leaf senescence (Sakuraba et al. 2013). In line with this, Arabidopsis *nol* mutants are able to degrade chlorophyll during senescence, while *nyc1* mutants exhibit a stay-green phenotype (Horie et al. 2009). Distinct roles for NYC1 and NOL seem also to exist in barley, while, by contrast, rice NOL and NYC1 were shown to act redundantly during leaf senescence (Kusaba et al. 2007; Sato et al. 2009).

The activity of the PAO/phyllobilin pathway in grass crops is further supported by the identification of a total of 13 different phyllobilins in a total of nine varieties from five cereal and forage crops, i.e. barley, wheat, sorghum, rice and ryegrass. These were identified and quantified by LC-MS analysis (Christ et al. 2016) and respective MS and MS/MS spectral data are accessible on our webpage (http://www.botinst.uzh.ch/en/research/physiology/horten/ms-library.html). This analysis showed some remarkable features of the second part of the PAO/phyllobilin pathway in Gramineae species. Thus, none of the phyllobilins identified here and in former work performed with maize (Berghold et al. 2006) is demethylated at the $O13^4$ position. This indicates that a functional homolog of MES16, known to be solely responsible for phyllobilin demethylation in Arabidopsis (Christ et al. 2012), is absent in grasses.

Besides this consistent lack of phyllobilin demethylation, phyllobilin C1-deformylation was highly variable among the investigated species, but rather consistent within the different barley and wheat varieties. Thus, DNCC abundance did not exceed 30% in wheat, while more than 50% of the phyllobilins were deformylated in barley. The extremes were sorghum, which exclusively produced non-deformylated NCCs, and ryegrass, where DNCCs were detected almost exclusively. This pointed to highly differing deformylating activities in these species.

Surprisingly also, CO, which in Arabidopsis inhibits phyllobilin deformylation (Christ et al. 2013), had no effect in the two tested grass species, i.e. barley and ryegrass. Two explanations for this observation are possible: (i) unlike in Arabidopsis (Fig. 7B), CO might not have reached the target CYP enzyme inside the grass leaf segments used for the inhibition experiment. CO enters leaves through stomata, which anatomically differ between dicots and monocots. However, and despite the fact that stomata are closed in the dark, O_2 obviously could diffuse into the leaves, as deduced from successful $^{18}O_2$ labeling experiments in barley (Fig. 3). Thus, likely also CO can enter through grass stomata under similar experimental conditions. (ii) While in Arabidopsis, CYP89A9 specifically catalyzes phyllobilin deformylation, this reaction may be executed by a different class of enzymes in grasses. These enzymes were insensitive to CO and thus likely would not contain a heme cofactor. Nevertheless, the C1 lactam oxygen present in DNCCs is derived from molecular oxygen, as deduced from $^{18}O_2$ labeling studies (Fig. 3). Possible candidates for such an activity could be cytosolic 2-oxoglutarate-dependent dioxygenases (Kawai et al. 2014), but further analysis is required to solve this riddle.

C18-dihydroxylated phyllobilins were commonly found in all species investigated in this work, however their relative abundance was very low in sorghum and ryegrass. Again, this points to high variability of the activity responsible for dihydroxylation in the different species. $^{18}O_2$ labeling experiments proved that both incorporated oxygen atoms derive from molecular oxygen, i.e. pointing to a possible dioxygenase-catalyzed mechanism. Dioxygenase-dependent dihydroxylation of alkenes is known from bacteria (Boyd et al. 2000; Boyd et al. 2005) and has been attributed to different classes of enzymes, such as Rieske-type oxygenases (Lee and Gibson 1996; Gally et al. 2015) and heme-containing peroxidases (Mutti 2012). The nature of the enzyme catalyzing phyllobilin dihydroxylation in grasses remains elusive. Very recently, an NCC, classified as NCC_1002 (Kuai et al. 2018), was identified in apple (*Malus domestica*), apricot (*Prunus armeniaca*) and plum (*Prunus domestica*). In NCC_1002, one of the C18-hydroxyl groups is additionally conjugated with a glucose moiety (Erhart et al. 2016; Mittelberger et al. 2017). Among the grass species investigated here only sorghum produced this phyllobilin. It will be interesting to investigate in the future whether glucosylation at $C8^2$ and C18 is catalyzed by the same glucosyltransferase; however, to date in none of the species that produce glycosylated phyllobilins, such as Arabidopsis (Pružinská et al. 2005; Christ et al. 2016) or *Nicotiana rustica* (Berghold et al. 2004), have the respective glucosyltransferases been identified.

The most remarkable finding of this work is the high variation among the investigated grass species concerning the fraction of degraded chlorophyll that is recovered in respective phyllobilins. It was recently established that in senescent Arabidopsis leaves around 60-70% of degraded chlorophyll is recovered in DNCCs and NCCs as the largest fraction of phyllobilins (Christ et al. 2016). The fate of the remaining 30-40% degraded chlorophyll remains elusive. Similarly, the major degradation products of chlorophyll in barley, classified here as NCC_678 and DNCC_666, were shown to account for only about 20% of degraded chlorophyll (Losey and Engel 2001), while in *C. japonicum* almost quantitative amounts are recovered in phyllobilins (Curty and Engel 1996). Early radiolabeling experiments in etiolated barley seedlings using ^{14}C-aminolevulinic acid, which specifically labels the porphyrin moiety of chlorophyll, had indicated the accumulation of several labeled compounds upon senescence induction (Peisker et al. 1990). This is in line with the identification in our work of a total of 8-9 DNCCs and NCCs in two barley varieties; however, their overall abundance does not exceed 30% of degraded chlorophyll, thus confirming earlier work (Losey and Engel 2001). Oxidized forms of NCCs (termed yellow and pink chlorophyll catabolites) that have been identified as minor phyllobilins in senescent leaves and fruits from different species (Ulrich et al. 2011; Moser et al. 2008; Roca et al. 2017; Mittelberger et al. 2017), were also present in the grass species investigated here, but only in trace amounts. With the exception of ryegrass, where about 70% of degraded chlorophyll was recovered in phyllobilins, none of the other three species accumulated more than 20% phyllobilins; noteworthy with high consistency within the four different investigated wheat varieties. It has been proposed in the past that in some cases chlorophyll might be degraded beyond the level of phyllobilins (Hörtensteiner 2006; Hörtensteiner and Kräutler 2011); however, up to date the ultimate fate of chlorophyll remains largely elusive. Monopyrrolic degradation products of chlorophyll have been proposed to accumulate in senescing barley leaves, but the same compounds were also found in non-senescent leaves of radish (*Raphanus sativus*) questioning their specific occurrence as products of chlorophyll degradation during senescence (Suzuki and Shioi 1999). Isotope-labeling of chlorophyll combined with the use of state-of-the-art LC-MS instruments has the potential to allow the identification of genuine low-molecular weight degradation products of chlorophyll that are distinct from the known phyllobilins. This effort is particularly demanded in species where phyllobilins are low abundant or almost absent, but where the

involvement of the PAO/phyllobilin pathway has experimentally been confirmed, such as barley (this work) or rice (Tang et al. 2011).

The great diversity of phyllobilins found within and across species and the fact that several side modifications require energy-consuming reactions has led to the idea that phyllobilins may have, so far unknown, biological roles (Kräutler 2016). However, Arabidopsis lines lacking phyllobilin-modifying enzymes do not exhibit obvious growth or developmental phenotypes (Christ et al. 2012; Christ et al. 2013; Hauenstein et al. 2016), challenging this assumption. The low abundance of phyllobilins observed in grass species may further challenge the idea of a biological function for phyllobilins, but may, in contrast, also indicate their consumption during execution of such a role. Further research is required to elucidate this aspect of chlorophyll breakdown.

Author contribution statement AD and SH designed the work, AD and BC performed the work, AD, BC and SH analyzed data, AD and SH wrote the manuscript.

Acknowledgement The authors are thankful to Sylvain Aubry for advice and critical reading the manuscript. This work was supported by grants from the European Union (Marie-Curie Initial Training Network #264394 *CropLife*) and the Swiss National Science Foundation (#31003A_149389/1).

Conflict of Interest The authors declare that they have no conflict of interest.

References

Altschul SF, Madden TL, Schaffer AA, Zhang JH, Zhang Z, Miller W, Lipman DJ (1997) Gapped BLAST and PSI-BLAST: a new generation of protein database search programs. Nucl Acids Res 25:3389-3402. doi:10.1093/nar/25.17.3389

Avice JC, Etienne P (2014) Leaf senescence and nitrogen remobilization efficiency in oilseed rape (*Brassica napus* L.). J Exp Bot 65:3813-3824. doi:10.1093/jxb/eru177

Bai Y, Han N, Wu JX, Yang YN, Wang JH, Zhu MY, Bian HW (2014) A transient gene expression system using barley protoplasts to evaluate microRNAs for post-transcriptional regulation of their target genes. Plant Cell Tiss Org Cult 119:211-219. doi:10.1007/s11240-014-0527-z

Berghold J, Eichmüller C, Hörtensteiner S, Kräutler B (2004) Chlorophyll breakdown in tobacco: on the structure of two nonfluorescent chlorophyll catabolites. Chem Biodivers 1:657-668. doi:10.1002/cbdv.200490057

Berghold J, Müller T, Ulrich M, Hörtensteiner S, Kräutler B (2006) Chlorophyll breakdown in maize: on the structure of two nonfluorescent chlorophyll catabolites. Monatsh Chem 137:751-763. doi:10.1007/s00706-006-0473-5

Boyd DR, Clarke D, Cleij MC, Hamilton JTG, Sheldrake GN (2000) Bacterial biotransformation of isoprene and related dienes. Monatsh Chem 131:673-685. doi:10.1007/s007060070096

Boyd DR, Sharma ND, Bowers NI, Brannigan IN, Groocock MR, Malone JE, McConville G, Allen CCR (2005) Biocatalytic asymmetric dihydroxylation of conjugated mono- and poly-alkenes to yield enantiopure cyclic *cis*-diols. Adv Synth Catal 347:1081-1089. doi:10.1002/adsc.200505033

Christ B, Hauenstein M, Hörtensteiner S (2016) A liquid chromatography-mass spectrometry platform for the analysis of phyllobilins, the major degradation products of chlorophyll in *Arabidopsis thaliana*. Plant J 88:505-518. doi:10.1111/tpj.13253

Breeze E, Harrison E, McHattie S, Hughes L, Hickman R, Hill C, Kiddle S, Kim YS, Penfold CA, Jenkins D, Zhang C, Morris K, Jenner C, Jackson S, Thomas B, Tabrett A, Legaie R, Moore JD, Wild DL, Ott S, Rand D, Beynon J, Denby K, Mead A, Buchanan-Wollaston V (2011) High-resolution temporal profiling of transcripts during *Arabidopsis* leaf senescence reveals a distinct chronology of processes and regulation. Plant Cell 23:873-894. doi:10.1105/tpc.111.083345

Buchanan-Wollaston V, Page T, Harrison E, Breeze E, Lim PO, Nam HG, Lin JF, Wu SH, Swidzinski J, Ishizaki K, Leaver CJ (2005) Comparative transcriptome analysis reveals significant differences in gene expression and signalling pathways between developmental and dark/starvation-induced senescence in Arabidopsis. Plant J 42:567-585. doi:10.1111/j.1365-313X.2005.02399.x

Christ B, Hörtensteiner S (2014) Mechanism and significance of chlorophyll breakdown. J Plant Growth Regul 33:4-20. doi:10.1007/s00344-013-9392-y

Christ B, Schelbert S, Aubry S, Süssenbacher I, Müller T, Kräutler B, Hörtensteiner S (2012) MES16, a member of the methylesterase protein family, specifically demethylates fluorescent chlorophyll catabolites during chlorophyll breakdown in Arabidopsis. Plant Physiol 158:628-641. doi:10.1104/pp.111.188870

Christ B, Süssenbacher I, Moser S, Bichsel N, Egert A, Müller T, Kräutler B, Hörtensteiner S (2013) Cytochrome P450 CYP89A9 is involved in the formation of major chlorophyll catabolites during leaf senescence in *Arabidopsis*. Plant Cell 25:1868-1880. doi:10.1105/tpc.113.112151

Clough SJ, Bent AF (1998) Floral dip: a simplified method for *Agrobacterium*-mediated transformation of *Arabidopsis thaliana*. Plant J 16:735-743. doi:10.1046/j.1365-313x.1998.00343.x

Curty C, Engel N (1996) Detection, isolation and structure elucidation of a chlorophyll *a* catabolite from autumnal senescent leaves of *Cercidiphyllum japonicum*. Phytochemistry 42:1531-1536. doi:10.1016/0031-9422(96)00155-0

Das A, Guyer L, Hörtensteiner S (2018) Chlorophyll and chlorophyll catabolite analysis by HPLC. Methods Mol Biol 1744:223-235. doi:10.1007/978-1-4939-7672-0_18

Distelfeld A, Avni R, Fischer AM (2014) Senescence, nutrient remobilization, and yield in wheat and barley. J Exp Bot 65:3783-3798. doi:10.1093/jxb/ert477

Emanuelsson O, Nielsen H, Von Heijne G (1999) ChloroP, a neural network-based method for predicting chloroplast transit peptides and their cleavage sites. Protein Sci 8:978-984. doi:10.1110/ps.8.5.978

Erhart T, Mittelberger C, Vergeiner C, Scherzer G, Holzner B, Robatscher P, Oberhuber M, Kräutler B (2016) Chlorophyll catabolites in senescent leaves of the plum tree (*Prunus domestica*). Chem Biodivers 13:1441-1453. doi:10.1002/cbdv.201600181

Farmer E, Mousavi S, Lenglet A (2013) Leaf numbering for experiments on long distance signalling in *Arabidopsis*. Protocol Exchange. doi:10.1038/protex.2013.071

Ferdous J, Li Y, Reid N, Langridge P, Shi BJ, Tricker PJ (2015) Identification of reference genes for quantitative expression analysis of microRNAs and mRNAs in barley under various stress conditions. PLoS One 10:e0118503. doi:10.1371/journal.pone.0118503

Fulkerson WJ, Donaghy DJ (2001) Plant-soluble carbohydrate reserves and senescence - key criteria for developing an effective grazing management system for ryegrass-based pastures: a review. Aust J Exp Agr 41:261-275. doi:10.1071/Ea00062

Gally C, Nestl BM, Hauer B (2015) Engineering Rieske non-heme iron oxygenases for the asymmetric dihydroxylation of alkenes. Angew Chem Int Edit 54:12952-12956. doi:10.1002/anie.201506527

Gray J, Janick-Bruckner D, Bruckner B, Close PS, Johal GS (2002) Light-dependent death of maize *lls1* cells is mediated by mature chloroplasts. Plant Physiol 130:1894-1907. doi:10.1104/pp.008441

Gray J, Wardzala E, Yang M, Reinbothe S, Haller S, Pauli F (2004) A small family of LLS1-related non-heme oxygenases in plants with an origin amongst oxygenic photosynthesizers. Plant Mol Biol 54:39-54. doi:10.1023/B:PLAN.0000028766.61559.4c

Gregersen PL, Culetic A, Boschian L, Krupinska K (2013) Plant senescence and crop productivity. Plant Mol Biol 82:603-622. doi:10.1007/s11103-013-0013-8

Guyer L, Salinger K, Krügel U, Hörtensteiner S (2018) Catalytic and structural properties of pheophytinase, the phytol esterase involved in chlorophyll breakdown. J Exp Bot 69:879–889. doi:10.1093/jxb/erx326

Guyer L, Schelbert Hofstetter S, Christ B, Silverstre Lira B, Rossi M, Hörtensteiner S (2014) Different mechanisms are responsible for chlorophyll dephytylation during fruit ripening and leaf senescence in tomato. Plant Physiol 166:44-56. doi:10.1104/pp.114.239541

Hauenstein M, Christ B, Das A, Aubry S, Hörtensteiner S (2016) A role for TIC55 as a hydroxylase of phyllobilins, the products of chlorophyll breakdown during plant senescence. Plant Cell 28:2510-2527. doi:10.1105/tpc.16.00630

Hellens R, Edwards EA, Leyland NR, Bean S, Mullineaux PM (2000) pGreen: a versatile and flexible binary Ti vector for *Agrobacterium*-mediated plant transformation. Plant Mol Biol 42:819-832. doi:10.1023/A:1006496308160

Horie Y, Ito H, Kusaba M, Tanaka R, Tanaka A (2009) Participation of chlorophyll *b* reductase in the initial step of the degradation of light-harvesting chlorophyll *a*/*b*-protein complexes in *Arabidopsis*. J Biol Chem 284:17449-17456. doi:10.1074/jbc.M109.008912

Hörtensteiner S (1998) NCC malonyltransferase catalyses the final step of chlorophyll breakdown in rape (*Brassica napus*). Phytochemistry 49:953-956. doi:10.1016/S0031-9422(98)00001-6

Hörtensteiner S (2006) Chlorophyll degradation during senescence. Annu Rev Plant Biol 57:55-77. doi:10.1146/annurev.arplant.57.032905.105212

Hörtensteiner S (2009) Stay-green regulates chlorophyll and chlorophyll-binding protein degradation during senescence. Trends Plant Sci 14:155-162. doi:10.1016/j.tplants.2009.01.002

Hörtensteiner S, Kräutler B (2011) Chlorophyll breakdown in higher plants. Biochim Biophys Acta 1807:977-988. doi:10.1016/j.bbabio.2010.12.007

Hörtensteiner S, Vicentini F, Matile P (1995) Chlorophyll breakdown in senescent cotyledons of rape, *Brassica napus* L.: enzymatic cleavage of phaeophorbide *a in vitro*. New Phytol 129:237-246. doi:10.1111/j.1469-8137.1995.tb04293.x

Hörtensteiner S, Wüthrich KL, Matile P, Ongania K-H, Kräutler B (1998) The key step in chlorophyll breakdown in higher plants. Cleavage of pheophorbide *a* macrocycle by a monooxygenase. J Biol Chem 273:15335-15339. doi:10.1074/jbc.273.25.15335

Jespersen D, Zhang J, Huang BR (2016) Chlorophyll loss associated with heat-induced senescence in bentgrass. Plant Sci 249:1-12. doi:10.1016/j.plantsci.2016.04.016

Jiang H, Li M, Liang N, Yan H, Wei Y, Xu X, Liu J, Xu Z, Chen F, Wu G (2007) Molecular cloning and function analysis of the *stay green* gene in rice. Plant J 52:197-209. doi:10.1111/j.1365-313X.2007.03221.x

Kawai Y, Ono E, Mizutani M (2014) Evolution and diversity of the 2-oxoglutarate-dependent dioxygenase superfamily in plants. Plant J 78:328-343. doi:10.1111/tpj.12479

Kräutler B (2014) Phyllobilins - the abundant bilin-type tetrapyrrolic catabolites of the green plant pigment chlorophyll. Chem Soc Rev 43:6227-6238. doi:10.1039/c4cs00079j

Kräutler B (2016) Breakdown of chlorophyll in higher plants - Phyllobilins as abundant, yet hardly visible signs of ripening, senescence, and cell death. Angew Chem Int Ed 55:4882-4907. doi:10.1002/anie.201508928

Kräutler B, Hörtensteiner S (2014) Chlorophyll breakdown: chemistry, biochemistry and biology. In: Ferreira GC, Kadish KM, Smith KM, Guilard R (eds) Handbook of Porphyrin Science - Chlorophyll, Photosynthesis and Bio-inspired Energy, vol 28. Handbook of

Porphyrin Science, vol 28. World Scientific Publishing, Singapore, pp 117-185. doi:10.1142/9789814407755_0021

Kräutler B, Jaun B, Bortlik K-H, Schellenberg M, Matile P (1991) On the enigma of chlorophyll degradation: the constitution of a secoporphinoid catabolite. Angew Chem Int Ed Engl 30:1315-1318. doi:10.1002/anie.199113151

Krupinska K, Haussühl K, Schäfer A, van der Kooij TA, Leckband G, Lorz H, Falk J (2002) A novel nucleus-targeted protein is expressed in barley leaves during senescence and pathogen infection. Plant Physiol 130:1172-1180. doi:10.1104/pp.008565

Kuai B, Chen J, Hörtensteiner S (2018) The biochemistry and molecular biology of chlorophyll breakdown. J Exp Bot 69:751–767. doi:10.1093/jxb/erx322

Kusaba M, Ito H, Morita R, Iida S, Sato Y, Fujimoto M, Kawasaki S, Tanaka R, Hirochika H, Nishimura M, Tanaka A (2007) Rice NON-YELLOW COLORING1 is involved in light-harvesting complex II and grana degradation during leaf senescence. Plant Cell 19:1362-1375. doi:10.1105/tpc.106.042911

Langmeier M, Ginsburg S, Matile P (1993) Chlorophyll breakdown in senescent leaves: demonstration of Mg-dechelatase activity. Physiol Plant 89:347-353. doi:10.1111/j.1399-3054.1993.tb00165.x

Lee K, Gibson DT (1996) Stereospecific dihydroxylation of the styrene vinyl group by purified naphthalene dioxygenase from *Pseudomonas* sp strain NCIB 9816-4. J Bacteriol 178:3353-3356. doi:10.1128/jb.178.11.3353-3356.1996

Lim PO, Kim HJ, Nam HG (2007) Leaf senescence. Annu Rev Plant Biol 58:115-136. doi:10.1146/annurev.arplant.57.032905.105316

Livak KJ, Schmittgen TD (2001) Analysis of relative gene expression data using real-time quantitative PCR and the $2^{-\Delta\Delta\ ^{C}T}$ method. Methods 25:402-408. doi:10.1006/meth.2001.1262

Losey FG, Engel N (2001) Isolation and characterization of a urobilinogenoidic chlorophyll catabolite from *Hordeum vulgare* L. J Biol Chem 276:27233-27236. doi:10.1074/jbc.M009288200

Mascher M, Gundlach H, Himmelbach A, Beier S, Twardziok SO, Wicker T, Radchuk V, Dockter C, Hedley PE, Russell J, Bayer M, Ramsay L, Liu H, Haberer G, Zhang XQ, Zhang Q, Barrero RA, Li L, Taudien S, Groth M, Felder M, Hastie A, Simkova H, Stankova H, Vrana J, Chan S, Munoz-Amatriain M, Ounit R, Wanamaker S, Bolser D, Colmsee C, Schmutzer

T, Aliyeva-Schnorr L, Grasso S, Tanskanen J, Chailyan A, Sampath D, Heavens D, Clissold L, Cao S, Chapman B, Dai F, Han Y, Li H, Li X, Lin C, McCooke JK, Tan C, Wang P, Wang S, Yin S, Zhou G, Poland JA, Bellgard MI, Borisjuk L, Houben A, Dolezel J, Ayling S, Lonardi S, Kersey P, Langridge P, Muehlbauer GJ, Clark MD, Caccamo M, Schulman AH, Mayer KFX, Platzer M, Close TJ, Scholz U, Hansson M, Zhang G, Braumann I, Spannagl M, Li C, Waugh R, Stein N (2017) A chromosome conformation capture ordered sequence of the barley genome. Nature 544:427-433. doi:10.1038/nature22043

Matsumoto T, Tanaka T, Sakai H, Amano N, Kanamori H, Kurita K, Kikuta A, Kamiya K, Yamamoto M, Ikawa H, Fujii N, Hori K, Itoh T, Sato K (2011) Comprehensive sequence analysis of 24,783 barley full-length cDNAs derived from 12 clone libraries. Plant Physiol 156:20-28. doi:10.1104/pp.110.171579

Meguro M, Ito H, Takabayashi A, Tanaka R, Tanaka A (2011) Identification of the 7-hydroxymethyl chlorophyll *a* reductase of the chlorophyll cycle in *Arabidopsis*. Plant Cell 23:3442-3453. doi:10.1105/tpc.111.089714

Meyer A, Eskandari S, Grallath S, Rentsch D (2006) AtGAT1, a high affinity transporter for γ-aminobutyric acid in *Arabidopsis thaliana*. J Biol Chem 281:7197-7204. doi:10.1074/jbc.M510766200

Mittelberger C, Yalcinkaya H, Pichler C, Gasser J, Scherzer G, Erhar T, Schumacher S, Holzner B, Janik K, Robatscher P, Müller T, Kräutler B, Oberhuber M (2017) Pathogen-induced leaf chlorosis: products of chlorophyll breakdown found in degreened leaves of Phytoplasma-infected apple (*Malus x domestica* Borkh.) and spricot (*Prunus armeniaca* L.) trees relate to the pheophorbide *a* oxygenase/phyllobilin pathway. J Agric Food Chem 65:2651-2660. doi:10.1021/acs.jafc.6b05501

Morita R, Sato Y, Masuda Y, Nishimura M, Kusaba M (2009) Defect in non-yellow coloring 3, an α/β hydrolase-fold family protein, causes a stay-green phenotype during leaf senescence in rice. Plant J 59:940-952. doi:10.1111/j.1365-313X.2009.03919.x

Moser S, Ulrich M, Müller T, Kräutler B (2008) A yellow chlorophyll catabolite is a pigment of the fall colours. Photochem Photobiol Sci 7:1577-1581. doi:10.1039/b813558d

Mühlecker W, Ongania K-H, Kräutler B, Matile P, Hörtensteiner S (1997) Tracking down chlorophyll breakdown in plants: elucidation of the constitution of a 'fluorescent' chlorophyll catabolite. Angew Chem Int Ed Engl 36:401-404. doi:10.1002/anie.199704011

Mutti FG (2012) Alkene cleavage catalysed by heme and nonheme enzymes: reaction mechanisms and biocatalytic applications. Bioinorg Chem Appl 2012:626909. doi:10.1155/2012/626909

Oberhuber M, Berghold J, Breuker K, Hörtensteiner S, Kräutler B (2003) Breakdown of chlorophyll: a nonenzymatic reaction accounts for the formation of the colorless "nonfluorescent" chlorophyll catabolites. Proc Natl Acad Sci USA 100:6910-6915. doi:10.1073/pnas.1232207100

Oberhuber M, Berghold J, Kräutler B (2008) Chlorophyll breakdown by a biomimetic route. Angew Chem Int Ed 47:3057-3061. doi:10.1002/anie.200705330

Ougham H, Hörtensteiner S, Armstead I, Donnison I, King I, Thomas H, Mur L (2008) The control of chlorophyll catabolism and the status of yellowing as a biomarker of leaf senescence. Plant Biol 10 (Suppl. 1):4-14. doi:10.1111/j.1438-8677.2008.00081.x

Park S-Y, Yu J-W, Park J-S, Li J, Yoo S-C, Lee N-Y, Lee S-K, Jeong S-W, Seo HS, Koh H-J, Jeon J-S, Park Y-I, Paek N-C (2007) The senescence-induced staygreen protein regulates chlorophyll degradation. Plant Cell 19:1649-1664. doi:10.1105/tpc.106.044891

Peisker C, Thomas H, Keller F, Matile P (1990) Radiolabelling of chlorophyll for studies on catabolism. J Plant Physiol 136:544-549. doi:10.1016/S0176-1617(11)80211-7

Pružinská A, Anders I, Aubry S, Schenk N, Tapernoux-Lüthi E, Müller T, Kräutler B, Hörtensteiner S (2007) In vivo participation of red chlorophyll catabolite reductase in chlorophyll breakdown. Plant Cell 19:369-387. doi:10.1105/tpc.106.044404

Pružinská A, Anders I, Tanner G, Roca M, Hörtensteiner S (2003) Chlorophyll breakdown: pheophorbide *a* oxygenase is a Rieske-type iron-sulfur protein, encoded by the *accelerated cell death 1* gene. Proc Natl Acad Sci USA 100:15259-15264. doi:10.1073/pnas.2036571100

Pružinská A, Tanner G, Aubry S, Anders I, Moser S, Müller T, Ongania K-H, Kräutler B, Youn J-Y, Liljegren SJ, Hörtensteiner S (2005) Chlorophyll breakdown in senescent Arabidopsis leaves: characterization of chlorophyll catabolites and of chlorophyll catabolic enzymes involved in the degreening reaction. Plant Physiol 139:52-63. doi:10.1104/pp.105.065870

Ren GD, Zhou Q, Wu SX, Zhang YF, Zhang LG, Huang JR, Sun ZF, Kuai BK (2010) Reverse genetic identification of CRN1 and its distinctive role in chlorophyll degradation in *Arabidopsis*. J Integr Plant Biol 52:496-504. doi:10.1111/j.1744-7909.2010.00945.x

Rentsch D, Martinoia E (1991) Citrate transport into barley mesophyll vacuoles - comparison with malate-uptake activity. Planta 184:532-537. doi:10.1007/BF00197903

Rios JJ, Perez-Galvez A, Roca M (2014) Non-fluorescent chlorophyll catabolites in quince fruits. Food Res Int 65:255-262. doi:10.1016/j.foodres.2014.03.063

Rios JJ, Roca M, Perez-Galvez A (2015) Systematic HPLC/ESI-high resolution-qTOF-MS methodology for metabolomic studies in nonfluorescent chlorophyll catabolites pathway. J Anal Methods Chem 2015:490627. doi:10.1155/2015/490627

Roca M, Rios JJ, Chahuaris A, Perez-Galvez A (2017) Non-fluorescent and yellow chlorophyll catabolites in Japanese plum fruits (*Prunus salicina*, Lindl.). Food Res Int 100:332-338. doi:10.1016/j.foodres.2017.07.029

Rodoni S, Mühlecker W, Anderl M, Kräutler B, Moser D, Thomas H, Matile P, Hörtensteiner S (1997) Chlorophyll breakdown in senescent chloroplasts. Cleavage of pheophorbide *a* in two enzymic steps. Plant Physiol 115:669-676. doi:10.1104/pp.115.2.669

Sakuraba Y, Kim YS, Yoo SC, Hörtensteiner S, Paek NC (2013) 7-Hydroxymethyl chlorophyll *a* reductase functions in metabolic channeling of chlorophyll breakdown intermediates during leaf senescence. Biochem Biophys Res Comm 430:32-37. doi:10.1016/j.bbrc.2012.11.050

Sakuraba Y, Park SY, Kim YS, Wang SH, Yoo SC, Hörtensteiner S, Paek NC (2014) Arabidopsis STAY-GREEN2 is a negative regulator of chlorophyll degradation during leaf senescence. Mol Plant 7:1288-1302. doi:10.1093/Mp/Ssu045

Sakuraba Y, Schelbert S, Park S-Y, Han S-H, Lee B-D, Besagni Andrès C, Kessler F, Hörtensteiner S, Paek N-C (2012) STAY-GREEN and chlorophyll catabolic enzymes interact at light-harvesting complex II for chlorophyll detoxification during leaf senescence in *Arabidopsis*. Plant Cell 24:507-518. doi:10.1105/tpc.111.089474

Sato Y, Moria R, Katsuma S, Nishimura M, Tanaka A, Kusaba M (2009) Two short-chain dehydrogenase/reductases, NON-YELLOW COLORING 1 and NYC1-LIKE, are required for chlorophyll *b* and light-harvesting complex II degradation during senescence in rice. Plant J 57:120-131. doi:10.1111/j.1365-313X.2008.03670.x

Schelbert S, Aubry S, Burla B, Agne B, Kessler F, Krupinska K, Hörtensteiner S (2009) Pheophytin pheophorbide hydrolase (pheophytinase) is involved in chlorophyll breakdown during leaf senescence in Arabidopsis. Plant Cell 21:767-785. doi:10.1105/tpc.108.064089

Schenk N, Schelbert S, Kanwischer M, Goldschmidt EE, Dörmann P, Hörtensteiner S (2007) The chlorophyllases AtCLH1 and AtCLH2 are not essential for senescence-related chlorophyll breakdown in *Arabidopsis thaliana*. FEBS Lett 581:5517-5525. doi:10.1016/j.febslet.2007.10.060

Schiltz S, Munier-Jolain N, Jeudy C, Burstin J, Salon C (2005) Dynamics of exogenous nitrogen partitioning and nitrogen remobilization from vegetative organs in pea revealed by ^{15}N in vivo labeling throughout seed filling. Plant Physiol 137:1463-1473. doi:10.1104/pp.104.056713

Schuler MA (1996) Plant cytochrome P450 monooxygenases. Critical Rev Plant Sci 15:235-284. doi:10.1080/07352689609701942

Shimoda Y, Ito H, Tanaka A (2016) Arabidopsis STAY-GREEN, Mendel's green cotyledon gene, encodes magnesium-dechelatase. Plant Cell 28:2147-2160. doi:10.1105/tpc.16.00428

Soreng RJ, Peterson PM, Romaschenko K, Davidse G, Zuloaga FO, Judziewicz EJ, Filgueiras TS, Davis JI, Morrone O (2015) A worldwide phylogenetic classification of the Poaceae (Gramineae). J Syst Evol 53:117-137. doi:10.1111/jse.12150

Stothard P (2000) The sequence manipulation suite: JavaScript programs for analyzing and formatting protein and DNA sequences. Biotechniques 28:1102-1104

Strain HH, Cope BT, Svec WA (1971) Analytical procedures for the isolation, identification, estimation and investigation of the chlorophylls. Methods Enzymol 23:452-476. doi:10.1016/S0076-6879(71)23118-9

Süssenbacher I, Christ B, Hörtensteiner S, Kräutler B (2014) Hydroxymethylated phyllobilins: A puzzling new feature of the dioxobilin branch of chlorophyll breakdown. Chem-Eur J 20:87-92. doi:10.1002/chem.201303398

Suzuki Y, Shioi Y (1999) Detection of chlorophyll breakdown products in the senescent leaves of higher plants. Plant Cell Physiol 40:909-915. doi:10.1093/oxfordjournals.pcp.a029622

Tanaka R, Hirashima M, Satoh S, Tanaka A (2003) The *Arabidopsis-accelerated cell death* gene *ACD1* is involved in oxygenation of pheophorbide *a*: inhibition of pheophorbide *a* oxygenase activity does not lead to the "stay-green" phenotype in *Arabidopsis*. Plant Cell Physiol 44:1266-1274. doi:10.1093/pcp/pcg172

Tanaka R, Tanaka A (2011) Chlorophyll cycle regulates the construction and destruction of the light-harvesting complexes. Biochim Biophys Acta 1807:968-976. doi:10.1016/j.bbabio.2011.01.002

Tang YY, Li MR, Chen YP, Wu PZ, Wu GJ, Jiang HW (2011) Knockdown of Os*PA*O and Os*RCCR1* cause different plant death phenotypes in rice. J Plant Physiol 168:1952-1959. doi:10.1016/j.jplph.2011.05.026

Uauy C, Distelfeld A, Fahima T, Blechl A, Dubcovsky J (2006) A NAC gene regulating senescence improves grain protein, zinc, and iron content in wheat. Science 314:1298-1301. doi:10.1126/science.1133649

Ulrich M, Moser S, Müller T, Kräutler B (2011) How the colourless 'nonfluorescent' chlorophyll catabolites rust. Chem-Eur J 17:2330-2334. doi:10.1002/chem.201003313

Van der Graaff E, Schwacke R, Schneider A, Desimone M, Flügge UI, Kunze R (2006) Transcription analysis of Arabidopsis membrane transporters and hormone pathways during developmental and induced leaf senescence. Plant Physiol 141:776-792. doi:10.1104/pp.106.079293

Wesley SV, Helliwell CA, Smith NA, Wang M, Rouse DT, Liu Q, Gooding PS, Singh SP, Abbot D, Stoutjesdijk PA, Robinson SP, Gleave AP, Green AG, Waterhouse PM (2001) Construct design for efficient, effective and high-throuput gene silencing in plants. Plant J 27:581-590. doi:10.1046/j.1365-313X.2001.01105.x

Wu S, Li Z, Yang L, Xie Z, Chen J, Zhang W, Liu T, Gao S, Gao J, Zhu Y, Xin J, Ren G, Kuai B (2016) NON-YELLOWING2 (NYE2), a close paralog of NYE1, plays a positive role in chlorophyll degradation in Arabidopsis. Mol Plant 9:624-627. doi:10.1016/j.molp.2015.12.016

Zhang J, Yu G, Wen W, Ma X, Xu B, Huang B (2016) Functional characterization and hormonal regulation of the *PHEOPHYTINASE* gene *LpPPH* controlling leaf senescence in perennial ryegrass. J Exp Bot 67:935-945. doi:10.1093/jxb/erv509

Zhang WY, Xu YC, Li WL, Yang L, Yue X, Zhang XS, Zhao XY (2014) Transcriptional analyses of natural leaf senescence in maize. PLoS One 9:e115617. doi:10.1371/journal.pone.0115617

Figure legends

Fig. 1. The PAO/phyllobilin pathway of chlorophyll breakdown. In the first part of the pathway, chlorophyll is converted to *p*FCC by the shown enzmes, while in the second part mostly species-specific modifications of different side positions of *p*FCC (indicated by arrows) occur that ultimately lead to a diversity of different phyllobilins (R^1-R^3 indicate the relevant modifications according to Table 1). Note, that an oxidative deformylation reaction at position C1 ultimately leads to DNCCs, while without this modification the ultimate products are NCCs. Note also that these modifications occur at the (D)FCC level and conversion to (D)NCCs is catalyzed by the acidic pH of the vacuole, where phylobilins are ultimately stored. Phyllobilin abbreviations: DFCCs, dioxobilin-type fluorescent chlorophyll catabolites; DNCCs, dioxobilin-type nonflurescent chlorophyll catabolites; FCCs, formyloxobilin-type fluorescent chlorophyll catabolites; *p*FCC, *primary* fluorescent chlorophyll catabolite. Enyzme abbreviations: HCAR, 7-hydroxy-chlorophyll a reductase; NOL, NYC1-like; NYC1, nonyellow coloring 1; PAO, pheophorbide a oxygenase; PPH, pheophytin pheophorbide hydrolase; RCCR, red chlorophyll catabolite reductase; SGR, stay-green. Pyrrole ring labeling and numbering of important atoms is shown in *p*FCC.

Fig. 2. MS (top) and MS/MS (bottom) spectra of selected novel phyllobilins detected in this work. Constitutional formulae, MS/MS fragmentation sites and respective fragment ions are shown. P^+, protonated precursor ion.

Fig. 3. Mass spectra of selected phyllobilins from barley leaves that were senesced under ambient atmosphere (top; $^{16}O_2$) or in heavy oxygen gas (bottom; $^{18}O_2$). Note that the incorporation of one ^{18}O atom increases the mass of the respective phyllobilin by two mass units. Thus, both DNCC_666 (top panel) and NCC_678 (bottom) contain up to four oxygen labels that are derived from molecular oxygen.

Fig. 4. Transient expression of CCE-GFP fusion constructs in barley mesophyll protoplasts. GFP and chlorophyll autofluorescence were examined by confocal laser scanning microscopy. Bar = 20 µm.

Fig. 5. Complementation of the stay-green phenotypes of Arabidopsis *pao1* (**a**, **c**) and *pph-1* (**b**, **d**) with *Hv*PAO and *Hv*PPH. respectively. **a**, **b**. Degradation of chlorophyll during the course of senescence. **b**, **d.** Accumulation of pheophorbide (**b**) and pheophytin (**d**), respectively, is reduced in the complementation lines. Data are mean values ± standard deviation of three biological replicates. Asterisks indicate significant difference to respective Col-0 values at the same time points according to Student's *t* test (**P*≤0.05; ***P*≤0.01; ****P*≤0.001). n.d., not detected.

Fig. 6. Characterization of the PAO/phyllobilin pathway in barley during dark-induced senescence (days of dark, dd). **a**, **b**. Inhibition of PAO activity by bipyridyl leads to a retardation of chlorophyll breakdown (**a**) and the accumulation of pheophorbide *a* (**b**). **c**. Expression of chlorophyll catabolic genes during senescence*. S40* is a senescence-control gene. **d**. PAO immuno blot analysis. Three biological replicates of protein extracts at the indicated times of senescence are shown. **b**, **c**. Data are mean values ± standard deviation of three biological replicates. Asterisks indicate significant difference to respective values at the time point 0 dd according to Student's *t* test (**P*≤0.05; ***P*≤0.01; ****P*≤0.001). n.d., not detected.

Fig. 7. Analysis of phyllobilin formation in different grass species. **a**. Relative abundance of DNCCs and NCCs in the investigated grass varieties after 8 days of dark (dd) senescence. **b**. Analysis of DNCC formation after 6 dd in a CO-containing atmosphere (50%, v/v). DNCC formation is inhibited in Arabidopsis Col-0, but not in barley var. GP and ryegrass var. CE. **c**. Fraction of degraded chlorophyll that is recovered in phyllobilins after 8 dd. Data are mean values ± standard deviation of three biological replicates. The asterisks in **b** indicate a significantly smaller fraction of DNCCs after CO-treatment as compared to the control according to Student's *t* test (****P*≤0.001). The following varieties were analyzed: barley: Golden Promise (GP), Baraka (BA); wheat: Chinese Spring (CS), Chancellor (CH), Kanzler (KA), Bobwhite (BW); ryegrass: Ceres (CE); rice: Nipponbare (NB), sorghum: E-Tian (ET).

Figure 1

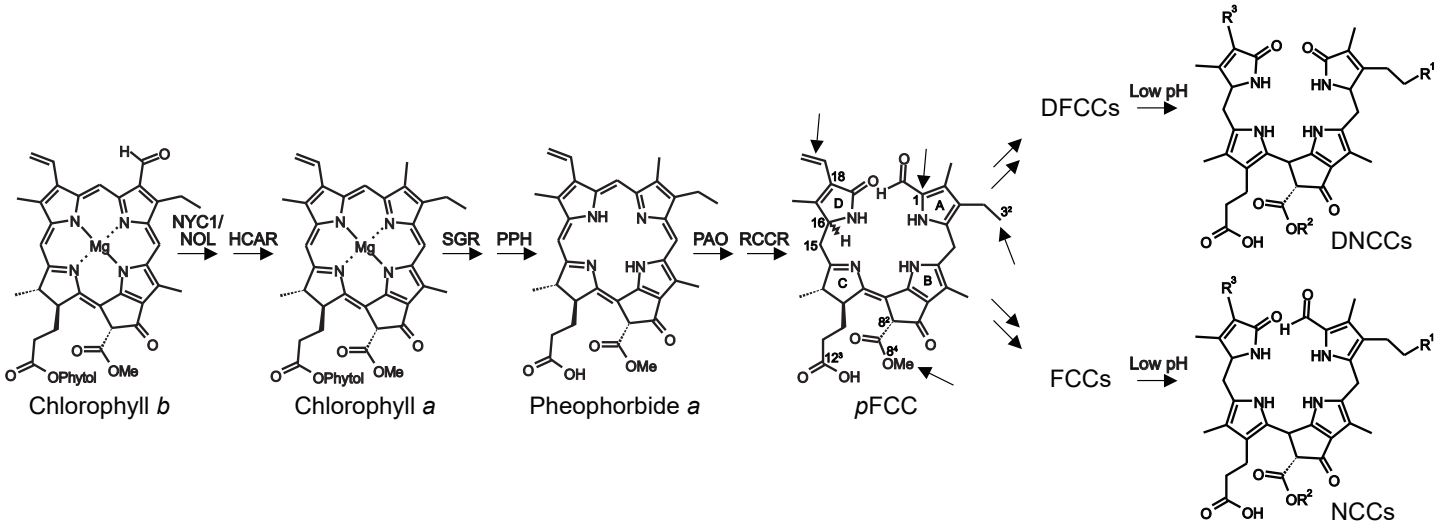

Fig. 1. The PAO/phyllobilin pathway of chlorophyll breakdown. In the first part of the pathway, chlorophyll is converted to *p*FCC by the shown enzmes, while in the second part mostly species-specific modifications of different side positions of *p*FCC (indicated by arrows) occur that ultimately lead to a diversity of different phyllobilins (R^1-R^3 indicate the relevant modifications according to Table 1). Note, that an oxidative deformylation reaction at position C1 ultimately leads to DNCCs, while without this modification the ultimate products are NCCs. Note also that these modifications occur at the (D)FCC level and conversion to (D)NCCs is catalyzed by the acidic pH of the vacuole, where phylobilins are ultimately stored. Phyllobilin abbreviations: DFCCs, dioxobilin-type fluorescent chlorophyll catabolites; DNCCs, dioxobilin-type nonflurescent chlorophyll catabolites; FCCs, formyloxobilin-type fluorescent chlorophyll catabolites; *p*FCC, *primary* fluorescent chlorophyll catabolite. Enyzme abbreviations: HCAR, 7-hydroxy-chlorophyll *a* reductase; NOL, NYC1-like; NYC1, nonyellow coloring 1; PAO, pheophorbide *a* oxygenase; PPH, pheophytin pheophorbide hydrolase; RCCR, red chlorophyll catabolite reductase; SGR, stay-green. Pyrrole ring labeling and numbering of important atoms is shown in *p*FCC.

Figure 2

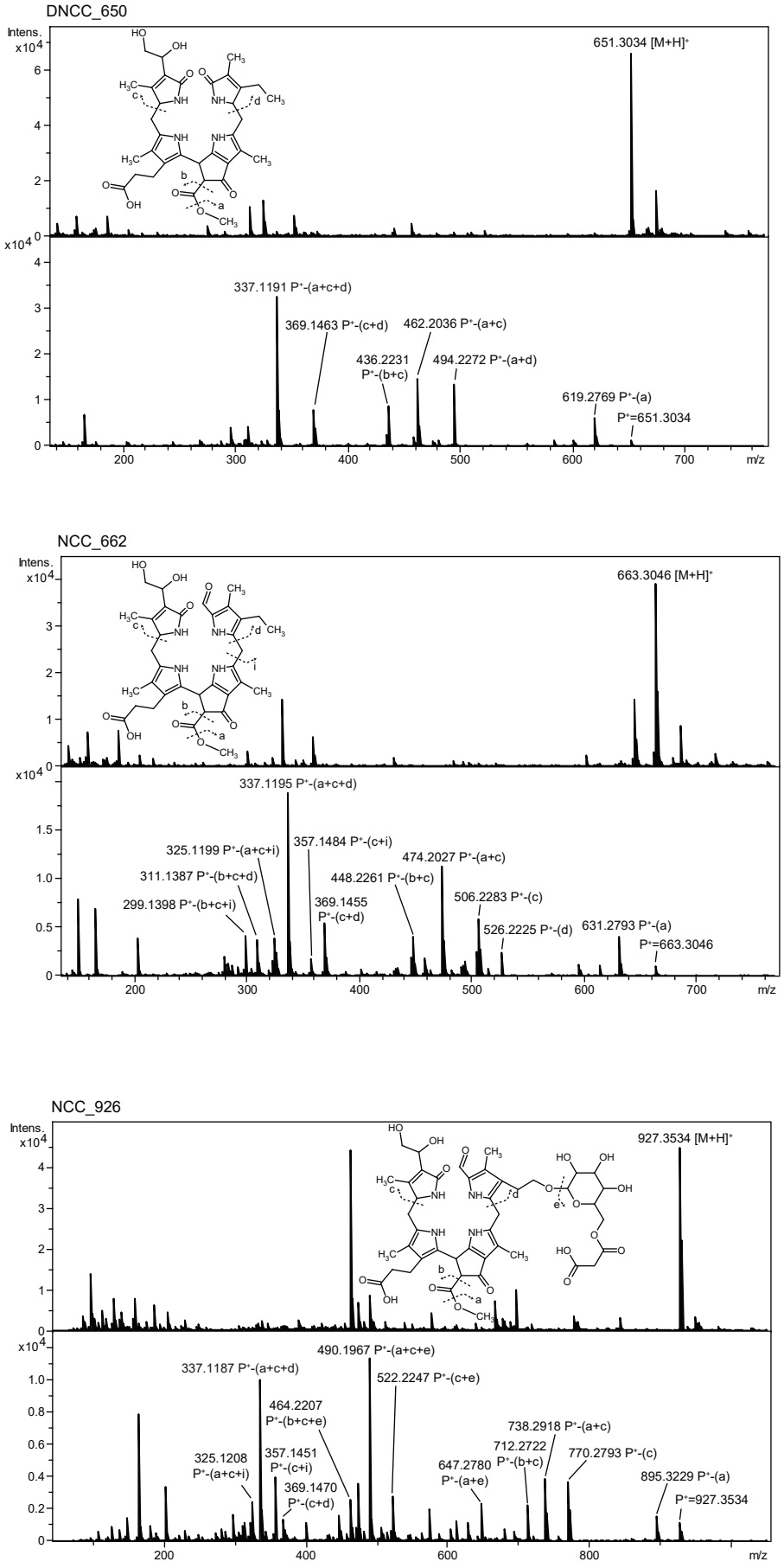

Fig. 2. MS (top) and MS/MS (bottom) spectra of selected novel phyllobilins detected in this work. Constitutional formulae, MS/MS fragmentation sites and respective fragment ions are shown. P^+, protonated precursor ion.

Figure 3

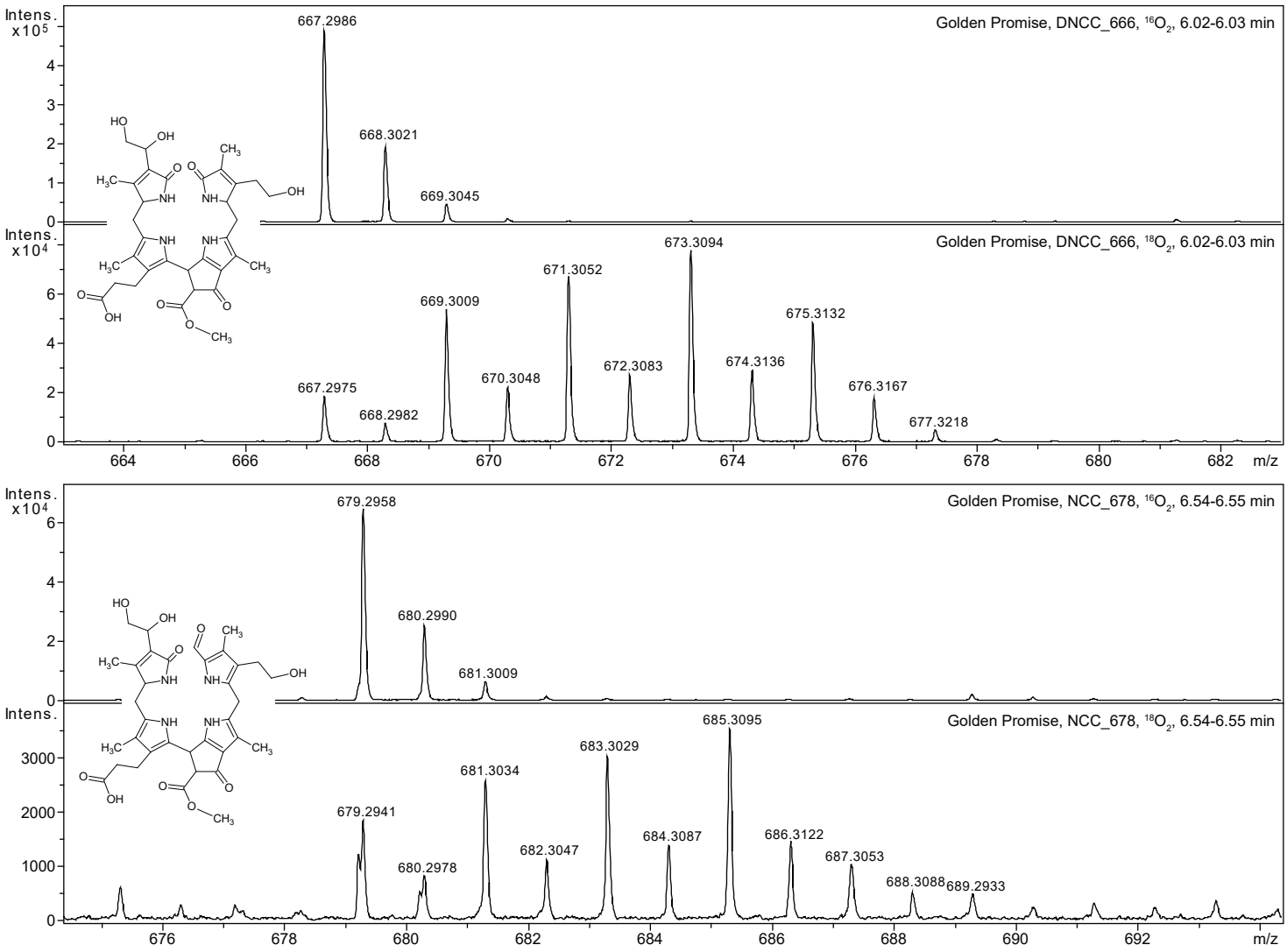

Fig. 3. Mass spectra of selected phyllobilins from barley leaves that were senesced under ambient atmosphere (top; $^{16}O_2$) or in heavy oxygen gas (bottom; $^{18}O_2$). Note that the incorporation of one ^{18}O atom increases the mass of the respective phyllobilin by two mass units. Thus, both DNCC_666 (top panel) and NCC_678 (bottom) contain up to four oxygen labels that are derived from molecular oxygen.

Figure 4

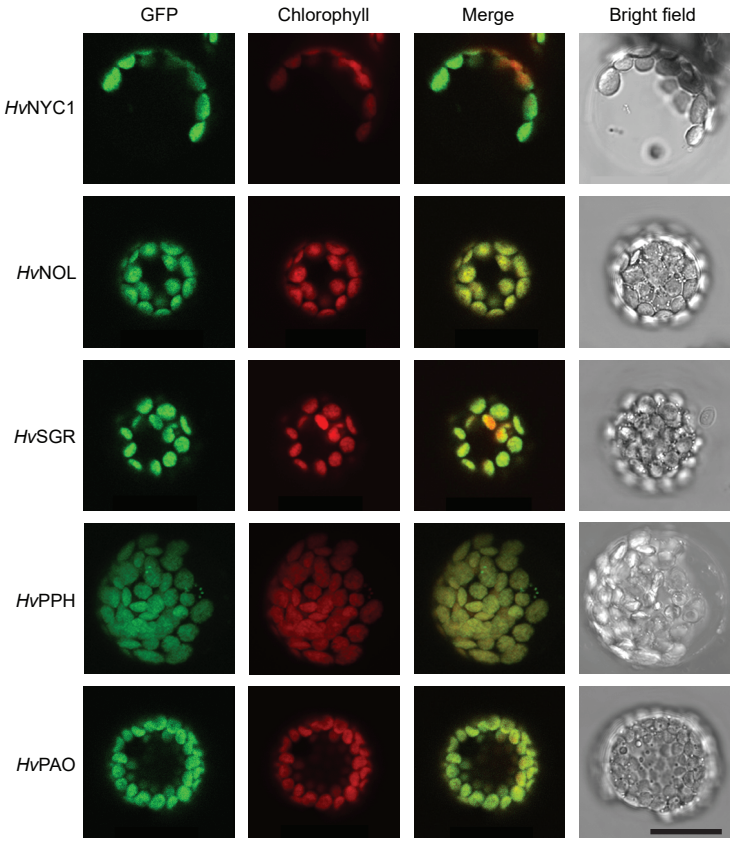

Fig. 4. Transient expression of CCE-GFP fusion constructs in barley mesophyll protoplasts. GFP and chlorophyll autofluorescence were examined by confocal laser scanning microscopy. Bar = 20 µm.

Figure 5

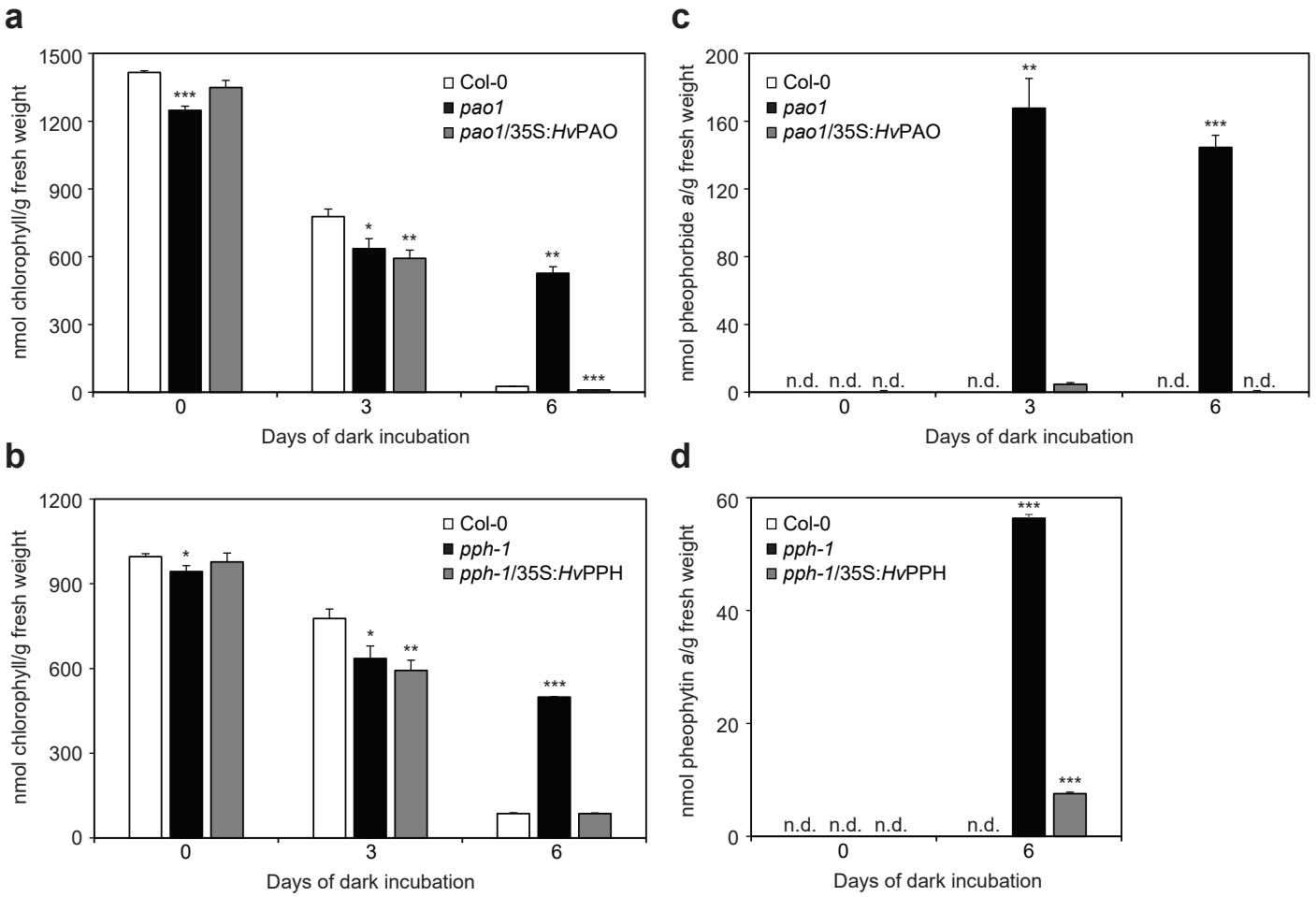

Fig. 5. Complementation of the stay-green phenotypes of Arabidopsis *pao1* (**a**, **c**) and *pph-1* (**b**, **d**) with *Hv*PAO and *Hv*PPH. respectively. **a**, **b**. Degradation of chlorophyll during the course of senescence. **b**, **d**. Accumulation of pheophorbide (**b**) and pheophytin (**d**), respectively, is reduced in the complementation lines. Data are mean values ± standard deviation of three biological replicates. Asterisks indicate significant difference to respective Col-0 values at the same time points according to Student's *t* test (**P* ≤0.05; ***P*≤0.01; ****P*≤0.001). n.d., not detected.

Figure 6

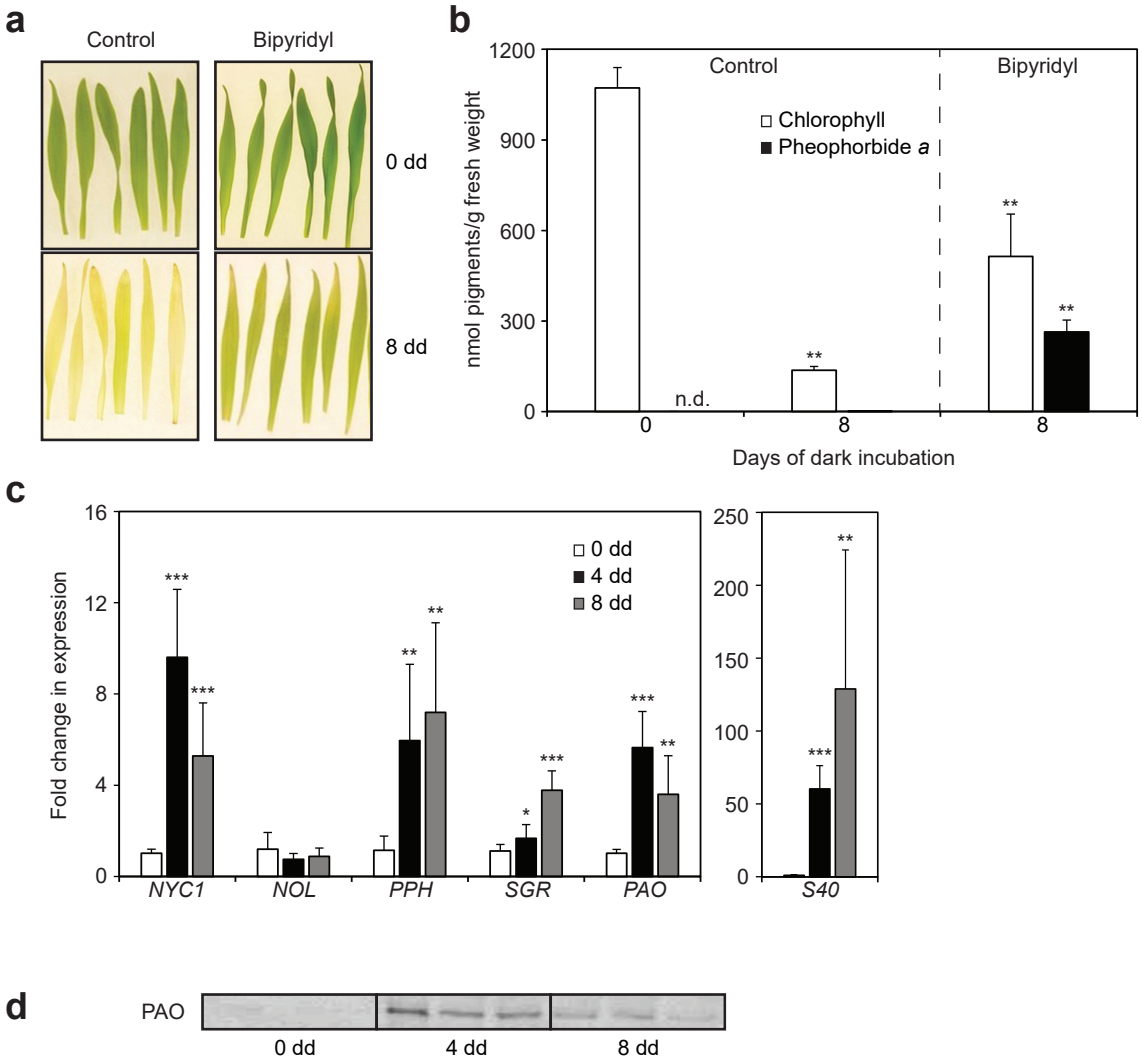

Fig. 6. Characterization of the PAO/phyllobilin pathway in barley during dark-induced senescence (days of dark, dd). **a**. **b**. Inhibition of PAO acitivity by bipyridyl leads to a retardation of chlorophyll breakdown (**a**) and the accumulation of pheophorbide *a* (**b**). **c**. Expression of chlorophyll catabolic genes during senescence. *S40* is a senescence-control gene. **d**. PAO immuno blot analysis. Three biological replicates of protein extracts at the indicated times of senescence are shown. **b**, **c**. Data are mean values ± standard deviation of three biological replicates. Asterisks indicate significant difference to respective values at the time point 0 dd according to Student's *t* test (**P*≤0.05; ***P*≤0.01; ****P*≤0.001). n.d., not

Figure 7

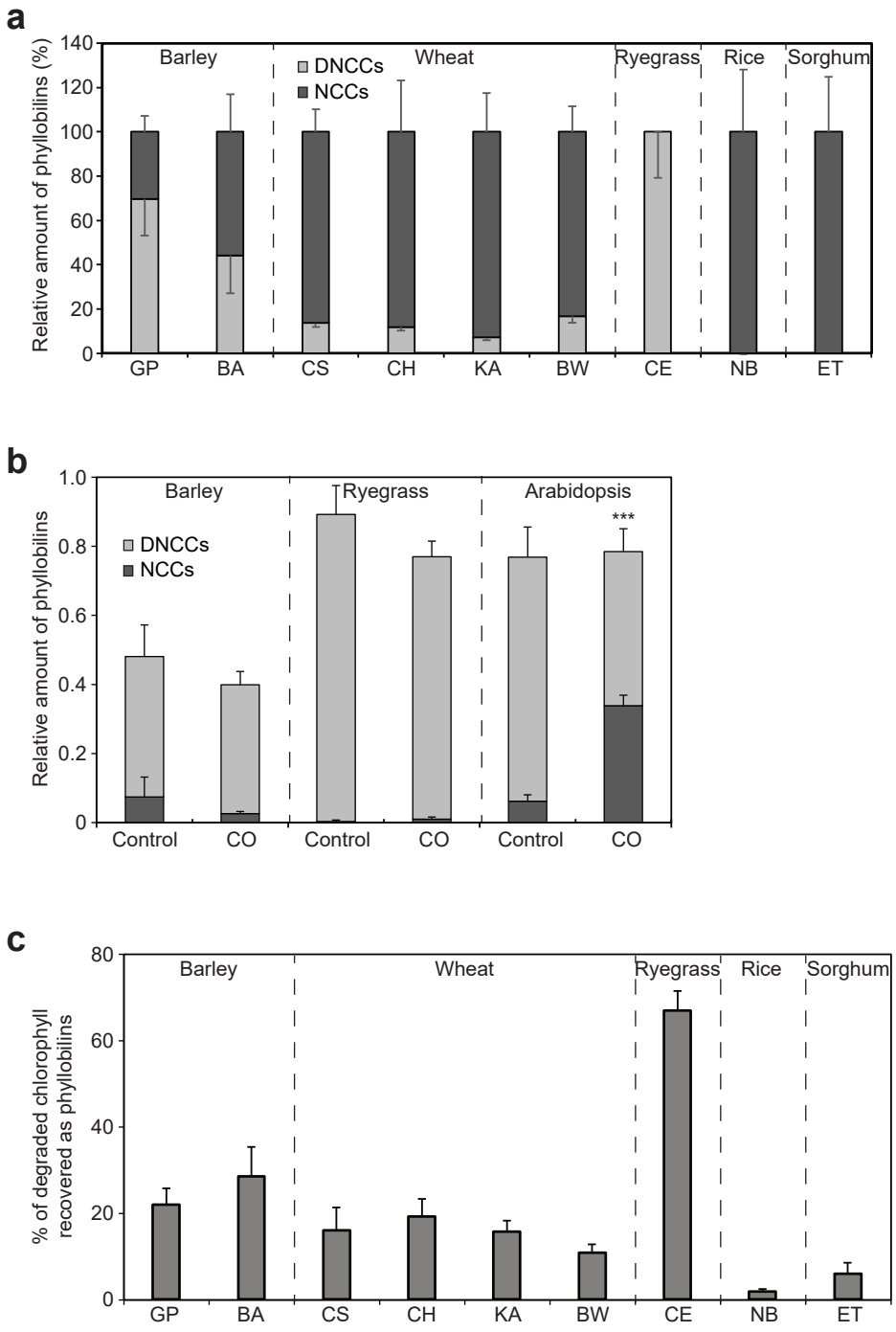

Fig. 7. Analysis of phyllobilin formation in different grass species. **a**. Relative abundance of DNCCs and NCCs in the investigated grass varieties after 8 days of dark (dd) senescence. **b**. Analysis of DNCC formation after 6 dd in a CO-containing atmosphere (50%, v/v). DNCC formation is inhibited in Arabidopsis Col-0, but not in barley var. GP and ryegrass var. CE. **c**. Fraction of degraded chlorophyll that is recovered in phyllobilins after 8 dd. Data are mean values ± standard deviation of three biological replicates. The asterisks in **b** indicate a significantly smaller fraction of DNCCs after CO-treatment as compared to the control according to Student's *t* test (***$P \leq 0.001$). The following varieties were analyzed: barley: Golden Promise (GP), Baraka (BA); wheat: Chinese Spring (CS), Chancellor (CH), Kanzler (KA), Bobwhite (BW); ryegrass: Ceres (CE); rice: Nipponbare (NB), sorghum: E-Tian (ET).

Supplemental material

Characterization of the PAO/phyllobilin pathway of chlorophyll breakdown in grasses

Aditi Das, Bastien Christ[1], Stefan Hörtensteiner[2]

Department of Plant and Microbial Biology, University of Zurich, Zollikerstrasse 107, CH-8008 Zurich, Switzerland

[1]Present address: Whitehead Institute, Massachusetts Institute of Technology, Cambridge, MA 02139-4307

[2]Address correspondence to shorten@botinst.uzh.ch

Supplemental Table S1: The barley homologs showing high sequence similarity with corresponding Arabidopsis gene products.

Gene name	**TAIR locus ID *(*Arabidopsis*)***	**GenBank ID**	***H. vulgare* clone name** (Matsumoto et al. 2011)
NYC	AT4G13250.1	AK356173.1	NIASHv1030P11
NOL	AT5G04900.1	AK369003.1	NIASHv2083K11
PPH	AT5G13800.2	AK364879.1	NIASHv2029B03
PAO	AT3G44880.1	AK353593.1	NIASHv1001F03
SGR	AT4G22920.1	AK356089.1	NIASHv1029O23

Supplemental Table S2: Primers used in this work

Gene name	Primer name	Primer sequence (5' → 3')
A GFP fusion constructs (restrictions sites bold)		
HvNYC1	NYC_F	CATGTA**ACTAGT**ATGGCCGCCGC
	NYC_R	ATCTGC**ACTAGT**TGTGCCAGGGAAAGG
HvNOL	NOL_F	GATCAT**ACTAGT**ATGGCCACCGTCGC
	NOL_R	TAGACA**AGATCT**GCATCCTCGGCAAC
HvPPH	PPH_F	GTATTC**ACTAGT**ATGGAAGTGGTTTCTTCAGC
	PPH_R	ATCTGC**ACTAGT**TCTGGACACTACCCGTAG
HvPAO	PAO_F	CATGTA**ACTAGT**ATGCCTACCGCCTCC
	PAO_R	GAATAC**AGATCT**ATATCAATGTCAGCGTG
HvSGR	SGR_F	CATGTA**ACTAGT**ATGGCCATCGCCGCTGC
	SGR_R	GAATAC**AGATCT**ATCTGCGGCGGCGCCTG
B Real-time PCR analyses		
HvNYC1	NYC_F_RT	GGAGTCGCCAAACCAGACA
	NYC_R_RT	CTTTGCCCCCTTCACAACAT
HvNOL	NOL_F_RT	CGCTCGCTCGCTCCAG
	NOL_R_RT	CGGGAAGAAGGCTGCGT
HvPPH	PPH_F_RT	AAGTGGCGATTCCTGGTCTG
	PPH_R_RT	CGCCTTGCTATTCTTGGTGC
HvPAO	PAO_F_RT	TACGACCGCCAGAAGCATTT
	PAO_R_RT	CACCACACCACATCCTCACA
HvSGR	SGR_RT_F	CGCGCCATACGATGACGAA
	SGR_RT_R	CCGGCGGGAAGCAGC
HvS40	S40_RT_F	CGACGGCGACGTCCGATGTA
	S40_RT_R	CTTTGAGCGTCCTCCCTTTGC
HvADP	ADP_RT_F	TCTCATGGTTGGTCTCGATG
	ADP_RT_R	GGATGGTGGTGACGATCTCT
C T-DNA confirmation		
pao-1	N14-RP	GGCTCACCTGACGCTTGGTTA
	N14-LP	CGACGGTGACAATTCAAAGGG
pph-1	95-RP	TGTACAGGTTATCGGTGAGCC
	95-LP	CTACCAATCCTGGACTCCTCC
T-DNA	LBb1.3	ATTTTGCCGATTTCGGAAC
D Recombinant *HvPPH* cloning (restrictions sites bold; point mutations red)		
End primer	*Hv* PPH_BamHI_f	GG**GATCC**GTGCTCTGTGTTGGGAGAGCTTC
	Hv PPH_SalI_r	CCC**GTCGAC**TCATCTGGACACTACCCG
F118S mutation	*Hv* PPH_F_inner	CGAGAAGTCTGGCACCAAGAATAGCAAGGC
	Hv PPH_R	GGTGCCAGACTTCTCGTAGTATACCGTCAGC
H261P mutation	*Hv* PPH_F	CCTTCCTAATCCTGCAAGATCTCCTCG
	Hv PPH_R_inner	GCAGGATTAGGAAGGAAACCCCAAAATGGC
E Complementation constructs (restrictions sites bold)		
PPH	PPH_F_BPHAN	CATGTA**CTCGAG**ATGGAAGTGGTTTCTTCC
	PPH_R_BPHAN	ATCTGC**GGATCC**TCATCTGGACACTAC
PAO	PAO_HAN_FOR	**CTCGAG**ATGCCTACCGCCTCCCTC
	PAO_HAN_REV	**AAGCTT**TCAATCAATGTCAGCGTGCAC

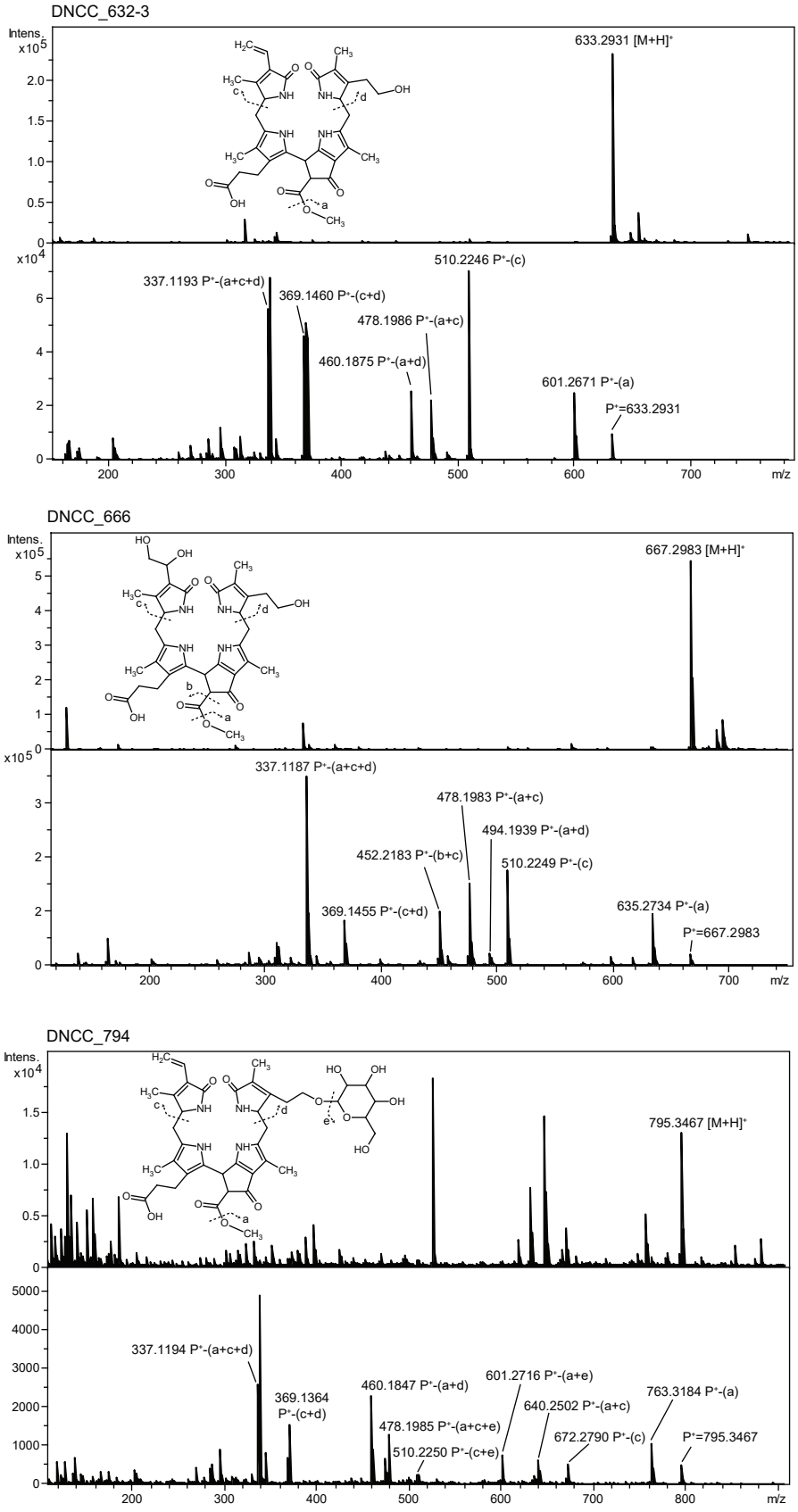

Supplemental Fig. S1. MS (top) and MS/MS (bottom) spectra of phyllobilins detected in this work. Constitutional formulae and MS/MS fragmentation sites and respective fragment ions are shown. P^+, protonated precursor ion. For further phyllobilins, see Fig. 2.

Supplemental Fig. S1 (continued)

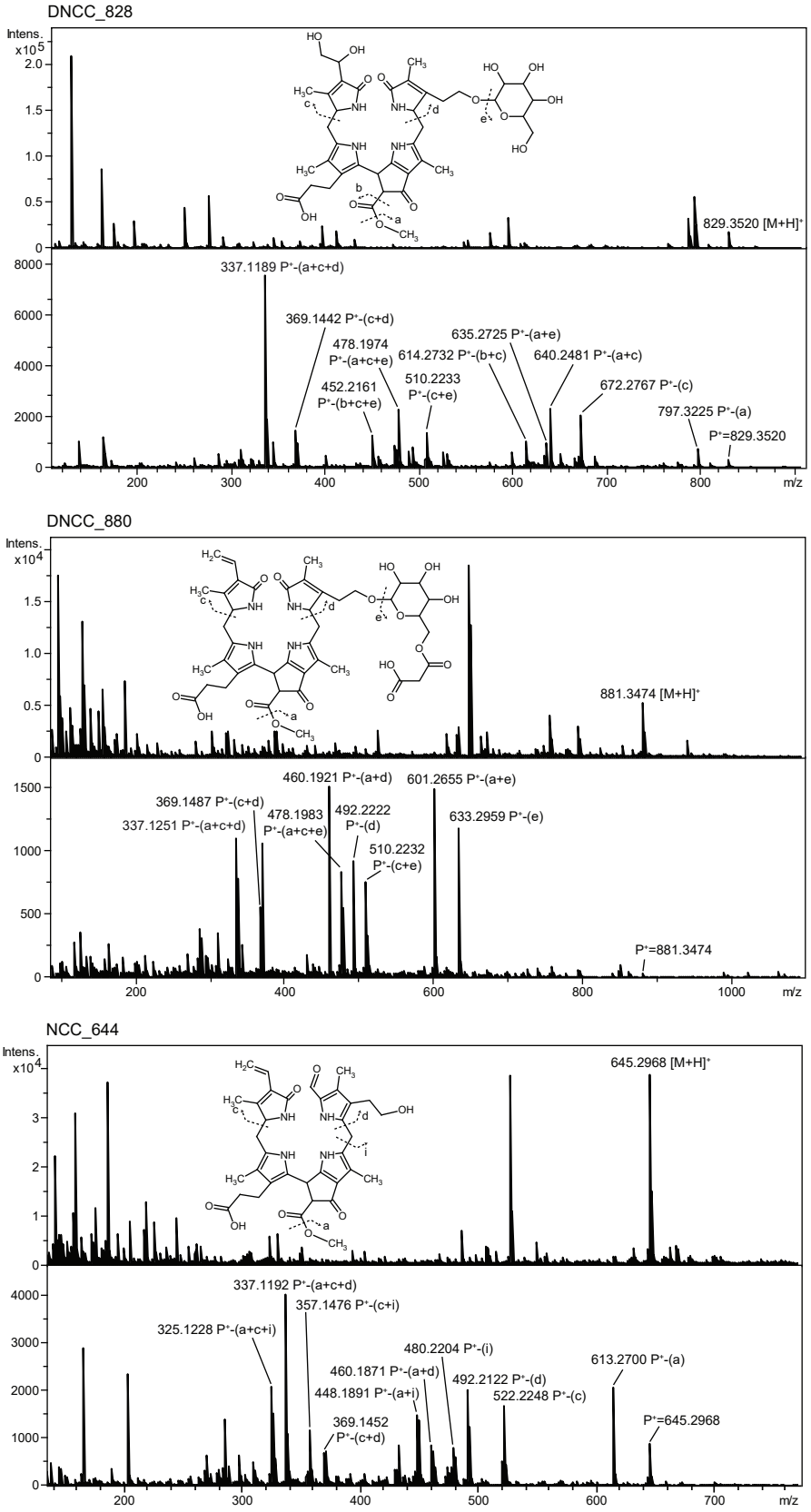

Supplemental Fig. S1 (continued)

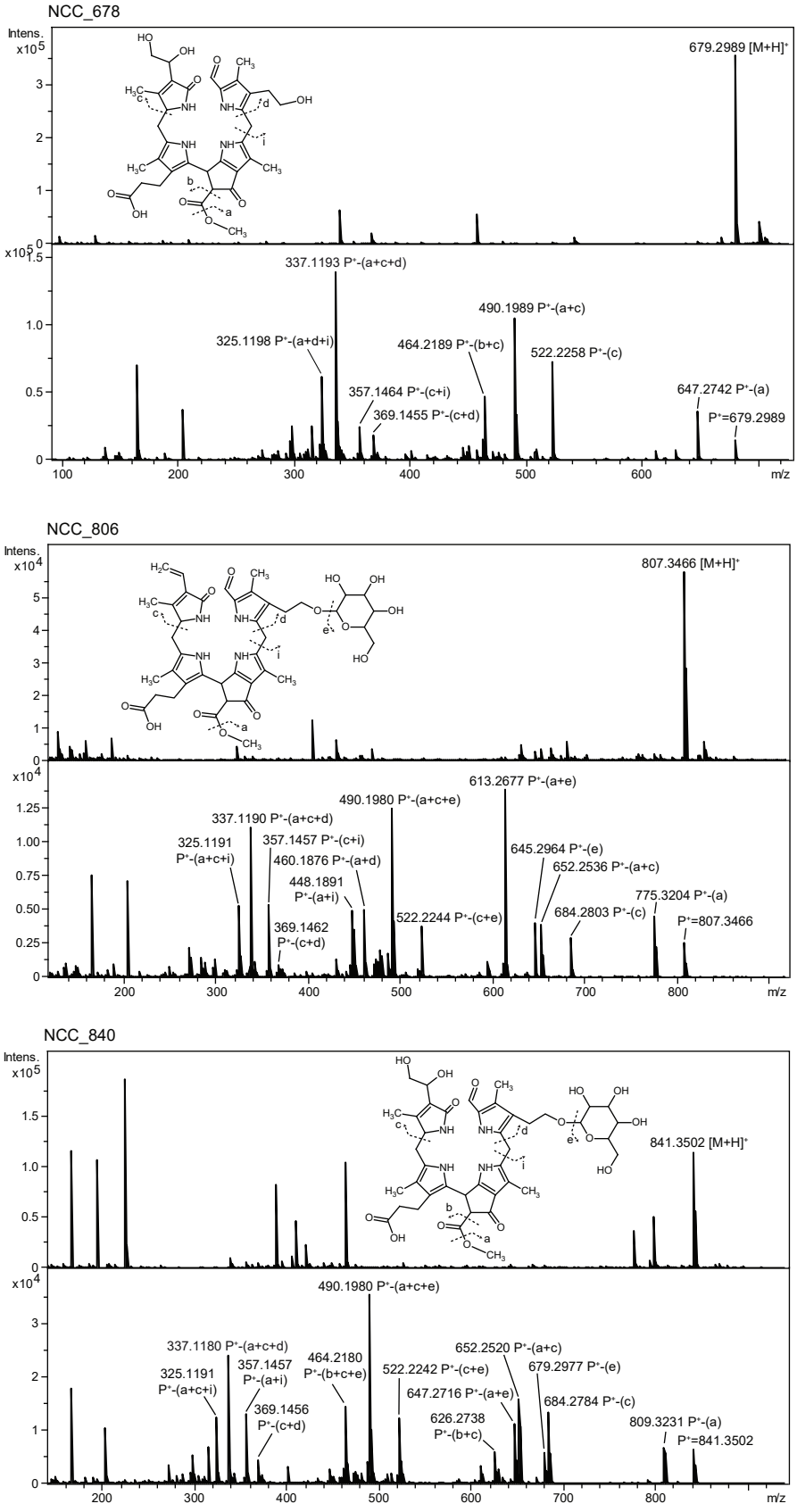

Supplemental Fig. S1 (continued)

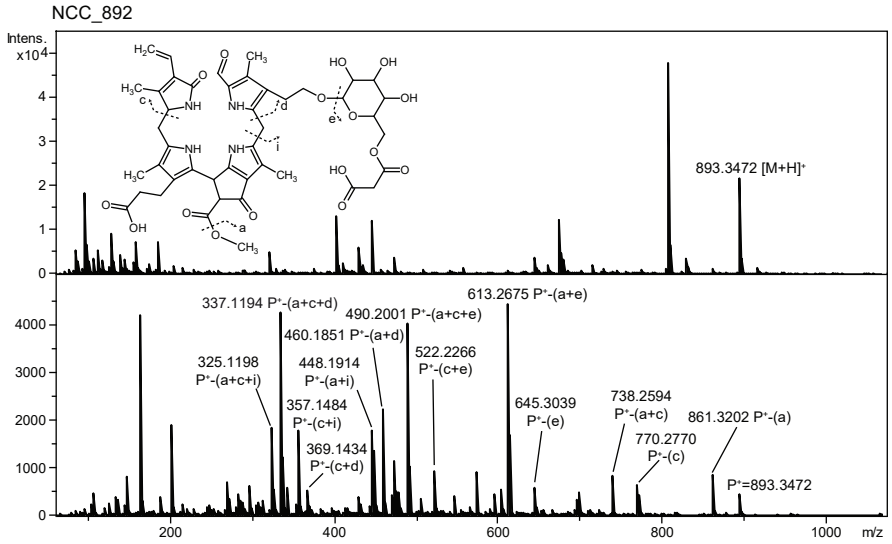

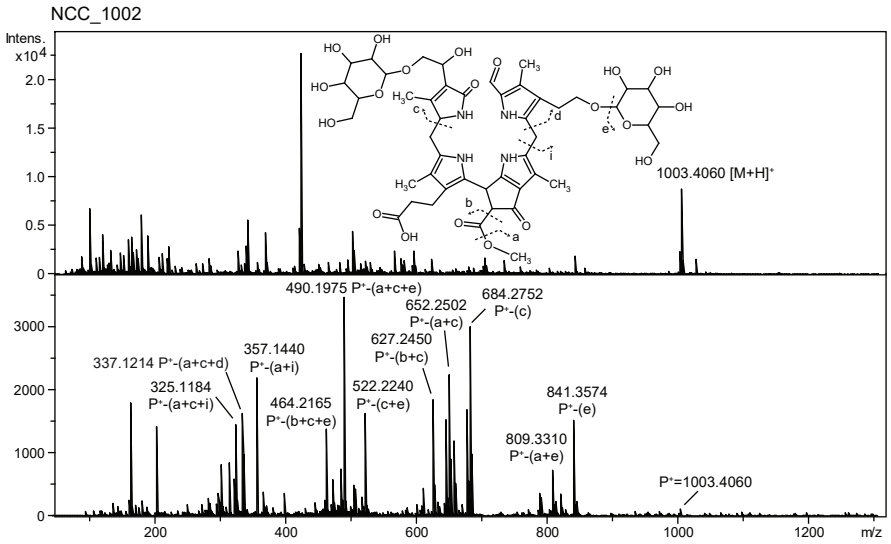

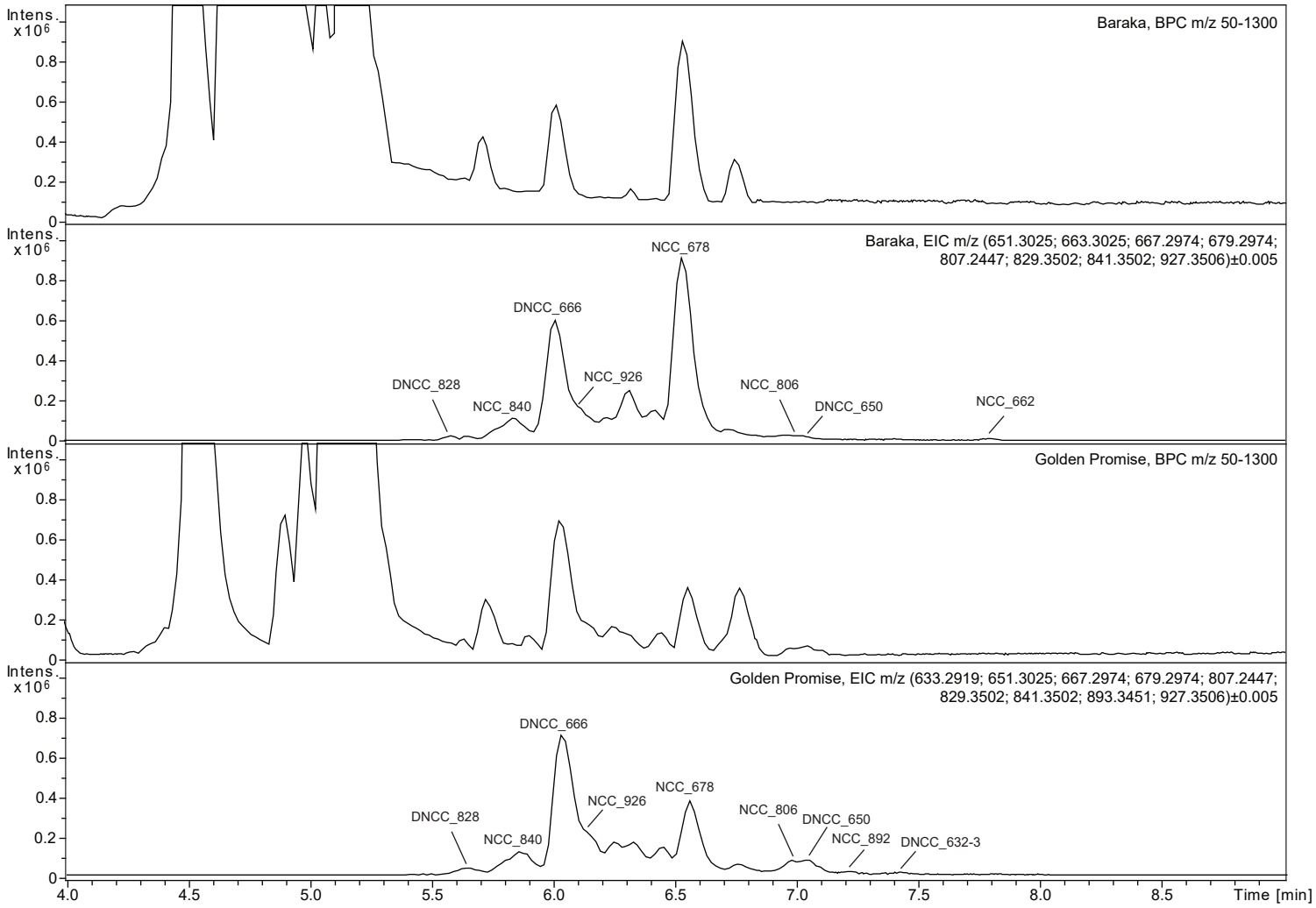

Supplemental Fig. S2. Base peak chromatograms (BPC) and extracted ion chromatograms (EICs) of the phyllobilins (see Table 1) detected in extracts of senescent leaves after 8 d in dark in two different barley varieties. For MS and MS/MS spectral details of the identified phyllobilins, see Fig. 2 and Supplemental Fig. S1.

a

Pair of species	*% identity (similarity) of CCEs*				
	NYC1	**NOL**	**PPH (*Hv*: 1/2)**	**PAO**	**SGR (*At*: 1/2)**
At vs. Hv	63.5 (76.3)	66.4 (75.6)	54.3 (67.8)/48.3 (59.3)	67.1 (76.3)	48.3 (54.3)/47.5 (56.8)
At vs. Os	63.1 (75.9)	65.9 (74.0)	54.3 (66.0)	66.7 (75.4)	51.2 (58.1)/50.7 (58.1)
Hs vs. Os	89.3 (92.9)	82.5 (86.5)	82.2 (87.6)/71.7 (76.4)	82.9 (89.6)	69.9 (74.7)

b

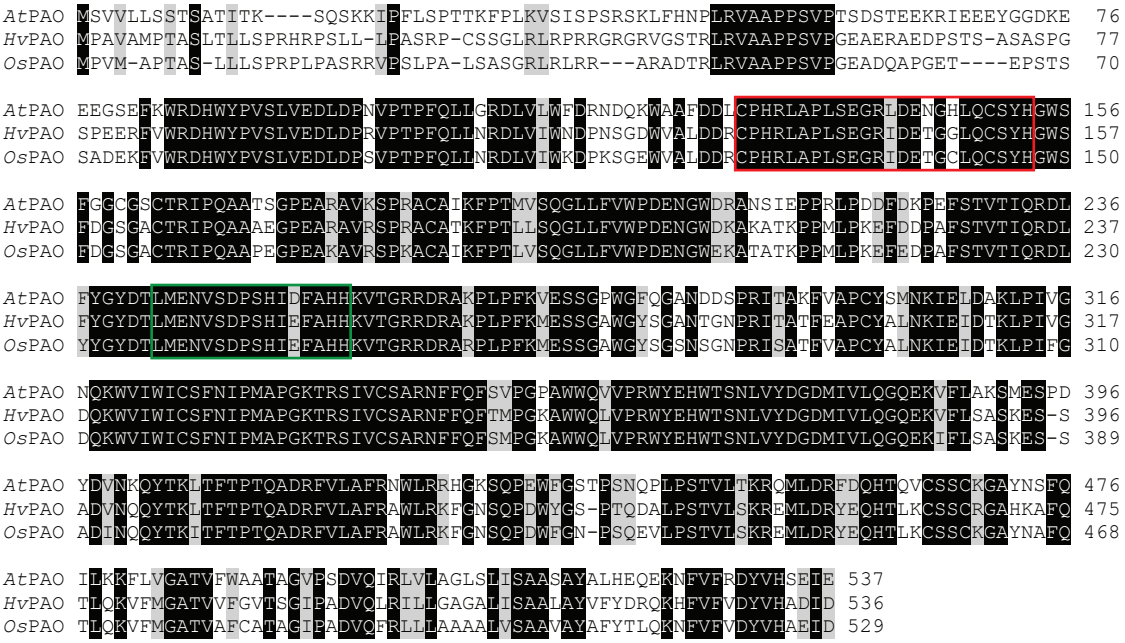

Supplemental Fig. S3. Analysis of chlorophyll catabolic enzymes (CCEs) from different species. **a**. Pairwise protein sequence identity of Arabidopsis, rice and barley CCEs. Note that two proteins are predicted for *Hv*PPH (see Fig. S4) and that Arabidopsis contains two SGRs. **b**. Alignment of PAO proteins. Important motifs are boxed: red, Rieske center; green, mononuclear iron-binding site. Residues that are identical or have conservative substitutions according to the Blosum 35 matrix in all three proteins are shaded in black and gray, respectively. GenBank protein sequence accession numbers used for sequence identity analysis and for sequence aligment are as follows: Arabidopsis (At): NYC1, NP_567400; NOL, NP_568145; PPH, BAH19780; PAO, NP_190074; SGR1, O82741; SGR2, Q66WT5. Barley (Hv): NYC1, BAJ87391; NOL, BAK00206; PPH1, BAK02426; PPH2, BAJ96082; PAO, BAJ85172; SGR, BAJ87307. Rice (Os): NYC1, XP_015621887; NOL, XP_015628274; PPH, XP_015643750; PAO, BAF10872; SGR, XP_015611682.

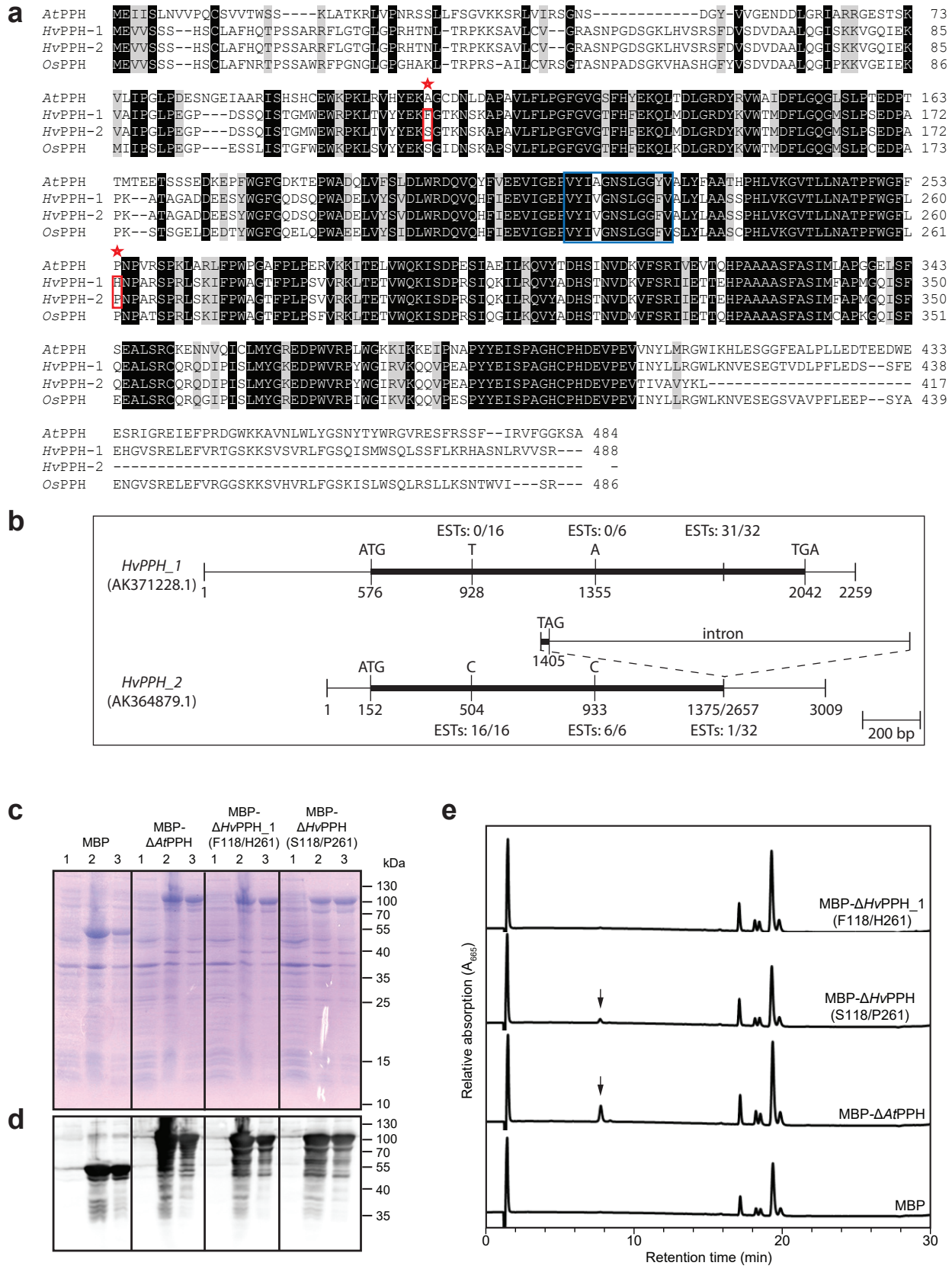

Supplemental Fig. S4. Analysis of barley PPH. **a**. Alignment of PPH proteins. Blue box, PPH motif; red boxes and asterisks, single amino acid substitutions of *Hv*PPHs as analyzed in panels **c**-**e**. Residues that are identical or have conservative substitutions according to the Blosum 35 matrix in all four shown proteins are shaded in black and gray, respectively. GenBank protein sequence accession numbers are as follows: *At*PPH, BAH19780; *Hv*PPH-1, BAK02426; *Hv*PPH-2, BAJ96082; *Os*PPH, XP_015643750. **b**. Graphical outline of the coding regions of *HvPPH_1* (AK371228.1) and *HvPPH_2* (AK364879.1). Note, that due to a likely mis-splicing event that is not well supported by ESTs, *HvPPH_2* has a premature stop codon. On the other hand, the two sequence variants T928 and A1355 of *HvPPH_1* are not supported by ESTs. **c**-**e**. Analysis of recombinant *Hv*PPH variants. Commassie-stained SDS gel (**c**) and MBP immunoblot (**d**) of *E. coli* extracts expressing empty pMal vector (MBP) or MBP-ΔPPH fusion proteins as shown. 1, cell extract before induction; 2, total cell extract after 3 h of induction with IPTG; 3, soluble protein fractions. For further details, see Materials and methods. **e**. HPLC analysis of enzyme assays after 30 min at 34 °C with soluble *E. coli* extracts containing recombinant MBP or MBP-ΔPPH proteins as shown using pheophytin *a* as substrate. Arrows indicate formed pheophorbide *a*.

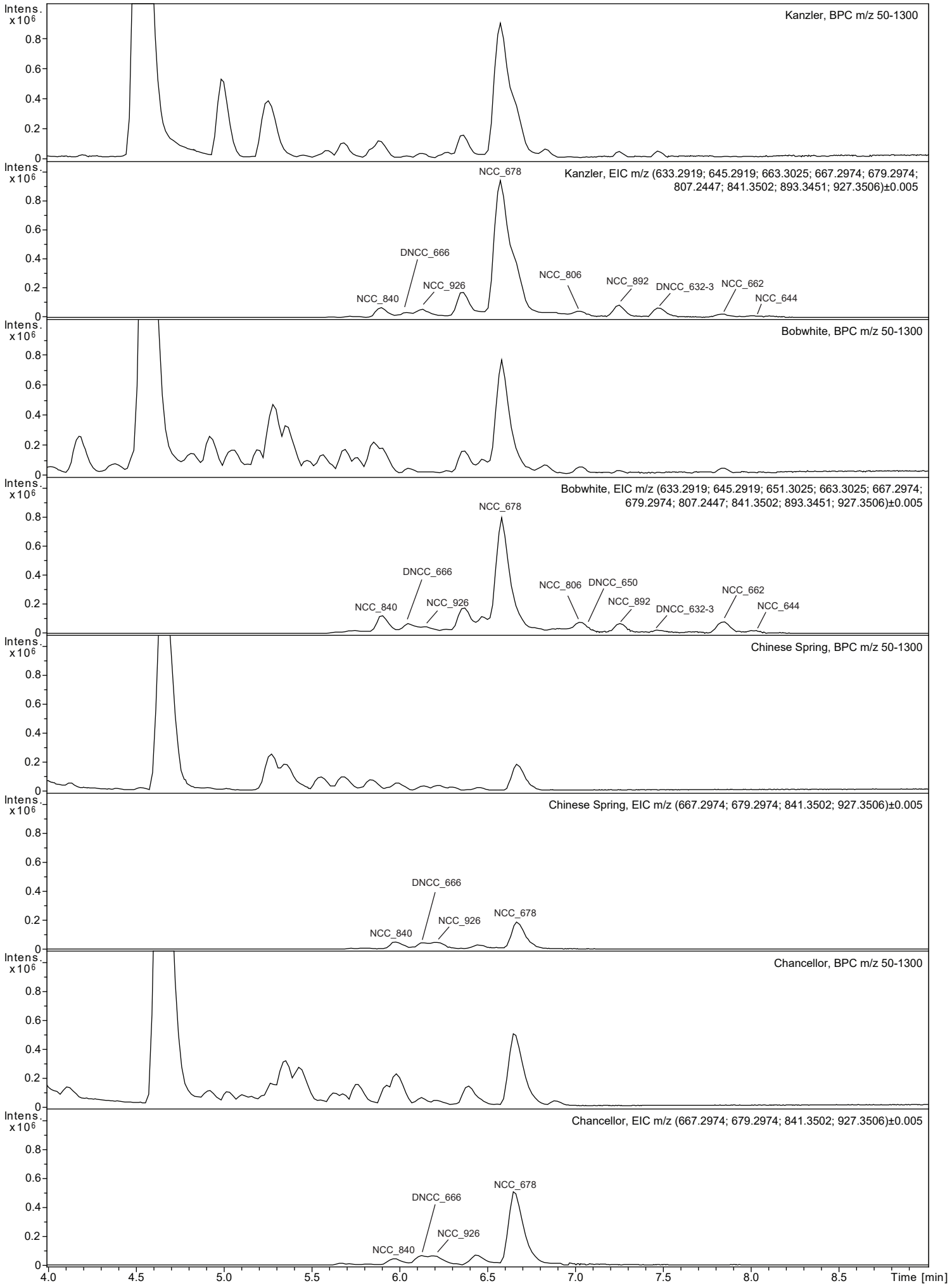

Supplemental Fig. S5. Base peak chromatograms (BPC) and extracted ion chromatograms (EICs) of the phyllobilins (see Table 1) detected in extracts of senescent leaves after 8 d in dark in four different wheat varieties. For MS and MS/MS spectral details of the identified phyllobilins, see Fig. 2 and Supplemental Fig. S1.

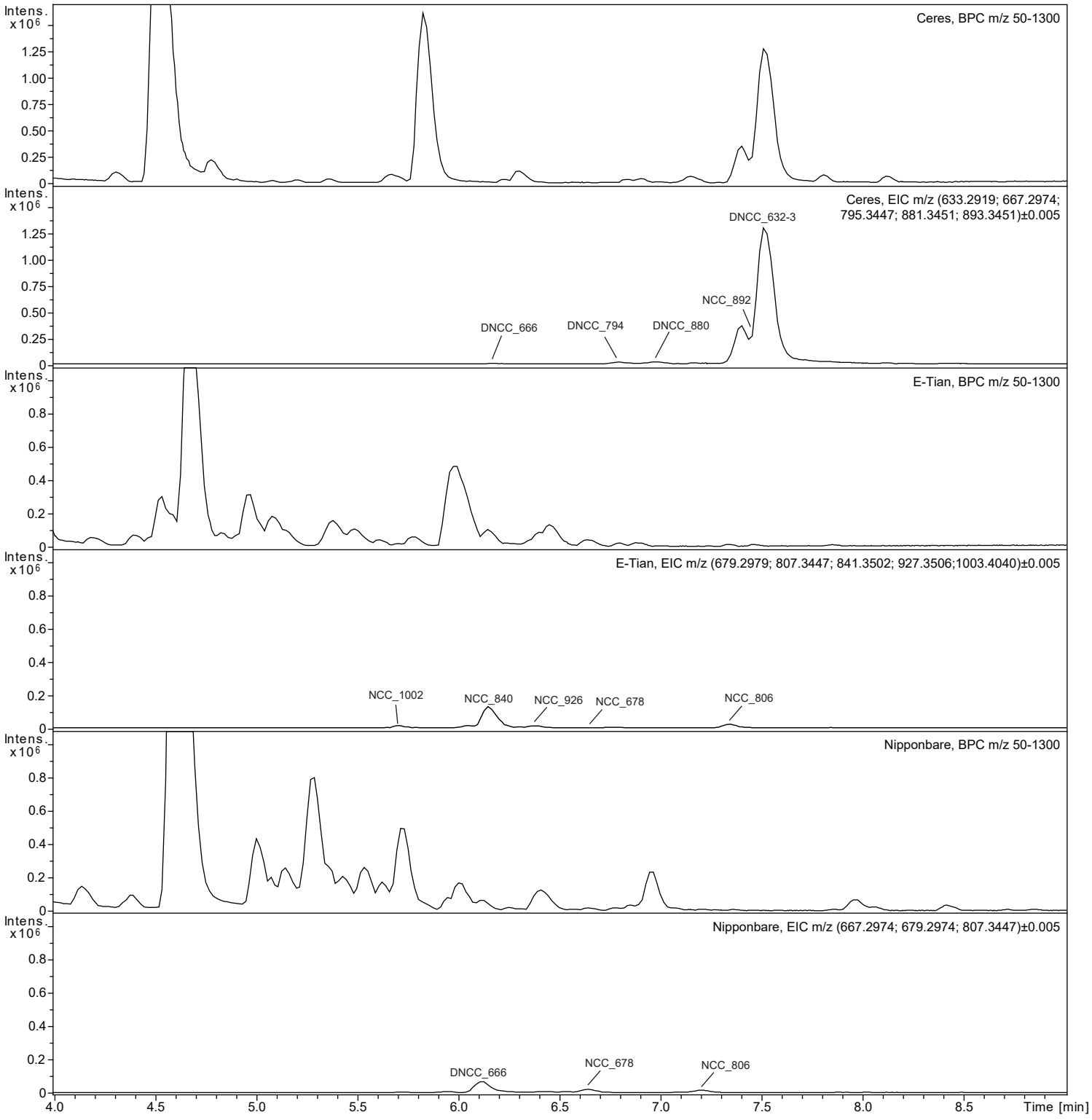

Supplemental Fig. S6. Base peak chromatograms (BPC) and extracted ion chromatograms (EICs) of the phyllobilins (see Table 1) detected in extracts of senescent leaves after 8 d in dark in rygreass var. Ceres, sorghum var. E-Tian and rice var. Nipponbare. For MS and MS/MS spectral details of the identified phyllobilins, see Fig. 2 and Supplemental Fig. S1.

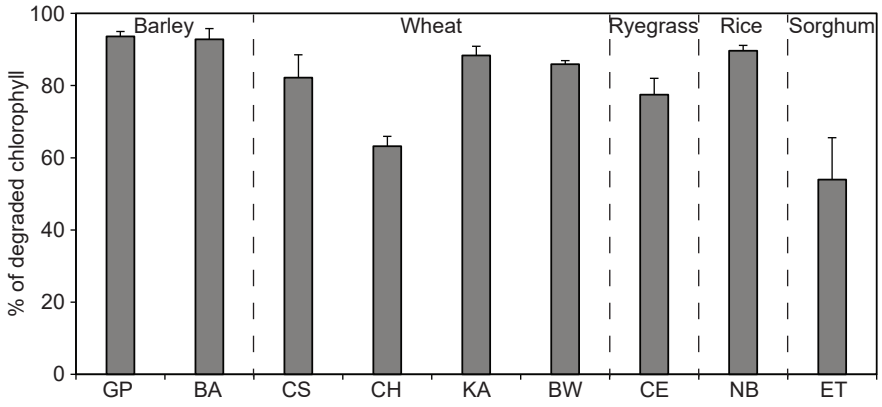

Supplemental Fig. S7. Analysis of chlorophyll degradation in different grass species. The relative amounts of degraded chlorophyll after 8 days of dark senescence are shown. The following varieties were analyzed: barley: Golden Promise (GP), Baraka (BA); wheat: Chinese Spring (CS), Chancellor (CH), Kanzler (KA), Bobwhite (BW); ryegrass: Ceres (CE); rice: Nipponbare (NB), sorghum: E-Tian (ET).